Prepared for submission to JHEP FERMILAB-PUB-12-078-T

Top-quark processes at NLO in production and decay

John M. Campbell and R. Keith Ellis
Fermilab, Batavia, IL 60510, USA
E-mails: johnmc@fnal.gov, ellis@fnal.gov.

Abstract: We describe the implementation of top production and decay processes in the parton-level Monte Carlo program MCFM. By treating the top quark as being on-shell, we can factorize the amplitudes for top-pair production, s-channel single-top production, and t-channel single-top production into the product of an amplitude for production and an amplitude for decay. In this way we can retain all spin correlations. Both the production and the decay amplitudes are calculated consistently at next-to-leading order in α_S. The full dependence on the b-quark mass is also kept. Phenomenological results are presented for various kinematic distributions at the LHC and for the top quark forward-backward asymmetry at the Tevatron.

Keywords: QCD, Hadron colliders, LHC

Contents

1 Introduction

The advent of the LHC has brought us data samples of top quarks more than an order of magnitude bigger than those observed at the Tevatron. Thus it is opportune to re-examine the issue of top quark physics to make sure that the theoretical treatment is at a level appropriate to confront this enlarged data sample. We have therefore decided to review the implementation of top processes in MCFM [1–4] with a view to providing the most sophisticated next-to-leading (NLO) treatment possible within the context of the top pole approximation.

It is now more than twenty five years since the first calculation of the NLO QCD corrections to the production of a pair of top quarks at a hadron collider [5]. This calculation, and subsequent NLO computations of single top production [6–12], provided predictions for stable top quarks, without consideration of their subsequent decay. This issue was addressed in Ref. [2], where the decay of the top quark was included for the case of single top production, incorporating also the effect of NLO QCD effects in the decay. For the case of top pair production, predictions including the decay of the top quark are now also available [3, 13–15]. Top pair production processes in association with a jet, including the decay, have been considered in ref. [16]. In order to consistently include corrections in the decay of the top quark it is imperative to also include the effect of NLO on the top quark width, a result that has been available for a long time [17]. In addition to these approaches, complete off-shell results for the final state produced by leptonic top quark pair decays, i.e. $pp \to \nu e^+ b e^- \bar{\nu} \bar{b}$, are also now available at NLO [18].

The purpose of this paper is to report in detail on a formalism to incorporate QCD NLO corrections in both production and decay, in a manner which is easily extensible to other top-production processes. We shall keep only the diagrams with a resonant top quark propagator, but provide a complete NLO treatment of both production and decay stages of the calculation. In particular we will include NLO corrections in the decay of the top quark, including from the hadronic decay of the W boson if appropriate, and retain for the first time the effects of a non-zero bottom quark mass. The price for including the b-mass effects is very modest in most of the calculation, due to the simple structure of the matrix elements [19]. Although the top quark is strictly on shell, we allow the consistent inclusion of the effects of an off-shell W-boson in top decay.

In this paper we will use this formalism to report on updated results for $t\bar{t}$ pair production, single top production with a W-boson exchanged in the t-channel, and single top production with a W-boson exchanged in the s-channel. However, as indicated above, the formalism should be easily extensible to more complicated processes such as $t\bar{t}H$, $t\bar{t}Z$ and $t\bar{t}W$. The lowest order diagrams for top pair production and decay are shown in Figure 1 and the lowest order diagrams for single-top production and decay are shown in Figure 2. The s-channel process has previously been treated in ref. [2], but now includes the b-quark mass consistently throughout. This paper is the first instance in which NLO corrections have been given for the t-channel single top production process in the four-flavour scheme with the decay of the top quark included. A four-flavour treatment of t-channel single top production without inclusion of the top quark decay has previously been given in refs. [11, 12]. The top-pair production process has the b-quark mass retained throughout, and in addition includes QCD radiative corrections to the W-boson decay for the case where the top quark decays hadronically.

The plan of this paper is as follows. In section 2 we review the results from the literature on the total width of the top quark, including mass corrections, off-shell W-boson corrections and NLO QCD corrections. Section 3 illustrates the method which we use to calculate top production amplitudes, by reference to the specific case of s-channel single top production. Section 4 presents the results on the amplitudes for top decay, both at the Born level and the NLO level including both real and virtual

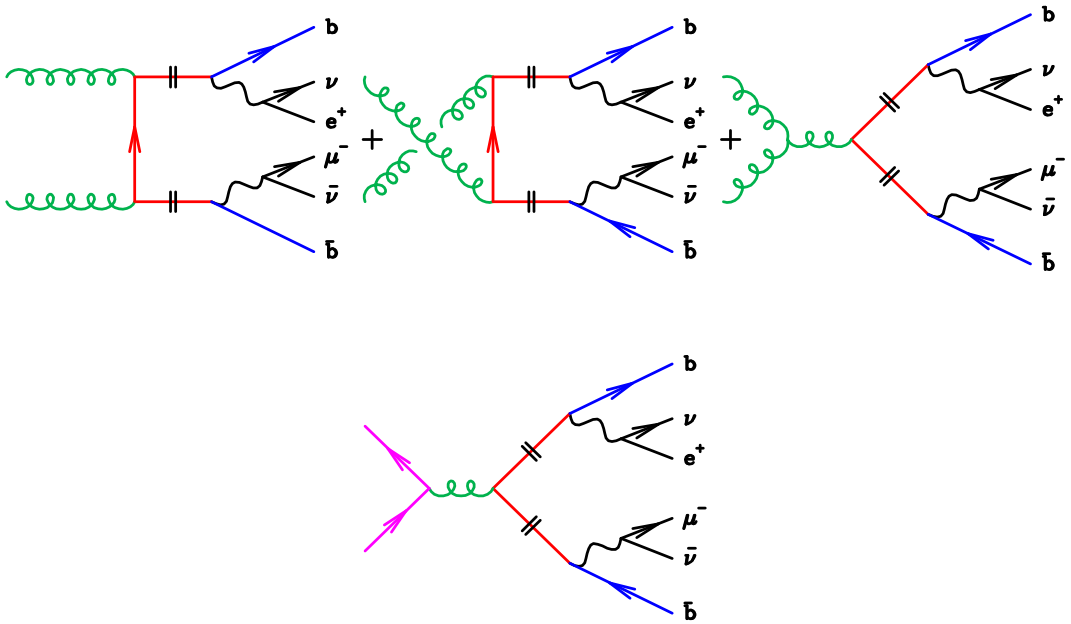

Figure 1. Lowest order diagrams for top-pair production and (semi-leptonic) decay. The double bars indicate that the top (anti-)quark is on shell.

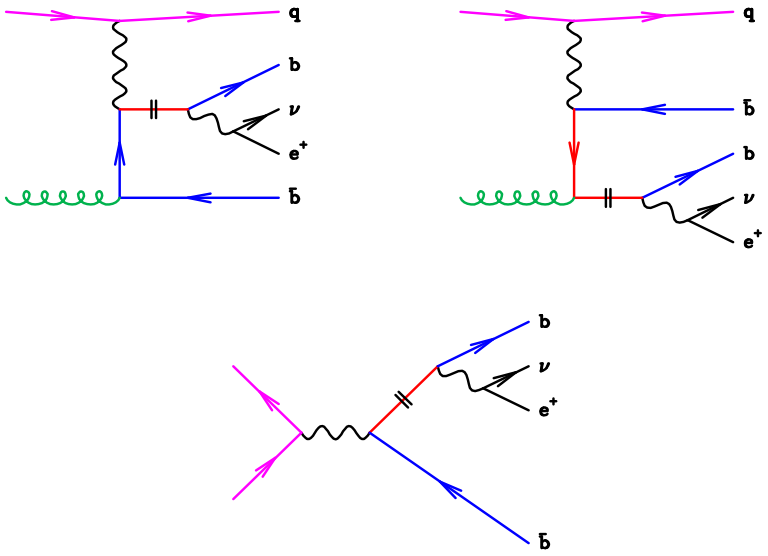

Figure 2. Lowest order diagrams for single-top production and (semi-leptonic) decay showing t-channel production (upper line) and s-channel production (lower line). The double bars indicate that the top quark is on shell.

corrections. In section 5 we present the counterterm that is used to handle the divergences that occur in the real gluon contribution to top decay and in section 6 we explain our procedure for ensuring that NLO effects are included consistently in top quark decay. Section 7 presents an illustration

$\beta = \frac{m_b}{m_t}$	$\omega^2 = \frac{p_W^2}{m_t^2}$,	$z = \frac{(p_t - p_W)^2}{m_t^2}$
$\xi = \frac{m_t^2}{m_W^2}$	$\gamma = \frac{\Gamma_W}{m_W}$	
$\lambda(x,y,z) = (x-y-z)^2 - 4yz$	$f = (1-\beta^2)^2 + \omega^2(1+\beta^2) - 2\omega^4$	$z_m = (1-\omega)^2$
$P_0(z) = \frac{1}{2}[1-\omega^2+z]$	$P_3(z) = \frac{1}{2}\sqrt{\lambda(1,\omega^2,z)}$	$W_0(z) = \frac{1}{2}[1+\omega^2-z]$
$P_+(z) = P_0 + P_3$	$P_-(z) = P_0 - P_3$	$Y_p(z) = \frac{1}{2}\ln\frac{P_+}{P_-}$
$W_+(z) = W_0 + P_3$	$W_-(z) = W_0 - P_3$	$Y_w(z) = \frac{1}{2}\ln\frac{W_+}{W_-}$

Table 1. Notation used for the calculation throughout this paper.

of phenomenological consequences for all three top production processes. The appendices contain a summary of the spinor notation used throughout this paper and present a complete calculation of the top quark width at NLO.

2 Results for the top quark width

In the limit of very large top mass (dropping the masses of the W and the b, s, d-quarks), the lowest order result for the top quark width is,

$$\Gamma^{(\infty)} = \frac{G_F m_t^3}{8\pi\sqrt{2}} \sum_j |V_{tj}|^2 \,. \tag{2.1}$$

As usual, G_F is the Fermi constant and V_{tj} are the CKM matrix elements for the $t \to j$ transitions. The superscript (∞) indicates that this is the result that would hold in the limit of infinite top mass, when the masses of the W-boson and bottom quark can be neglected. In the following we shall assume $V_{tb} = 1, V_{ts} = V_{td} = 0$. In this approximation the finite mass corrections implicit in the functions f and $\bar{P}_3$ correct this result as follows,

$$\Gamma_0(\omega^2) = \Gamma^{(\infty)} 2\bar{P}_3 f \,. \tag{2.2}$$

The notation used in this equation and throughout this paper, taken from ref. [20], is laid out in Table 1. Many of the quantities in Table 1 are functions of the variable z which is defined as,

$$z = \frac{(p_t - p_W)^2}{m_t^2} \,, \tag{2.3}$$

where p_t and p_W are the momenta of the top and the W-boson respectively. For the specific case of the lowest order process we have that $z = \beta^2$, corresponding to the b-quark being on shell. The variables that depend on z, when evaluated for $z = \beta^2$, are denoted with a bar. Thus we have,

$$P_3(\beta^2) \equiv \bar{P}_3 = \frac{1}{2}\sqrt{\lambda(1,\omega^2,\beta^2)} \,, \tag{2.4}$$

where the function λ is also defined in Table 1. We note that in the presence of one-gluon emission we have $z_m > z > \beta^2$.

The top-quark width is subject to higher order corrections due to gluon radiation,

$$\Gamma_t = \Gamma_0(\omega^2) + \alpha_S \Gamma_1(\omega^2)\,. \tag{2.5}$$

The result for the correction to the width has been given in ref. [17] and in ref. [20][1],

$$\begin{aligned}
\alpha_S\Gamma_1(\omega^2) \;=\; & \Gamma^{(\infty)}\frac{\alpha_S}{2\pi}C_F \times \\
& \Bigg\{ 8f\bar{P}_0\Big[\mathrm{Li}_2(1-\bar{P}_-) - \mathrm{Li}_2(1-\bar{P}_+) - 2\,\mathrm{Li}_2\left(1-\frac{\bar{P}_-}{\bar{P}_+}\right) + \bar{Y}_p \ln\left(\frac{4\bar{P}_3^2}{\bar{P}_+^2\bar{W}_+}\right) + \bar{Y}_w \ln\bar{P}_+\Big] \\
& + 4(1-\beta^2)\big[(1-\beta^2)^2 + \omega^2(1+\beta^2) - 4\omega^4\big]\bar{Y}_w \\
& + \big[3-\beta^2+11\beta^4-\beta^6+\omega^2(6-12\beta^2+2\beta^4) - \omega^4(21+5\beta^2) + 12\omega^6\big]\bar{Y}_p \\
& + 8f\bar{P}_3 \ln\left(\frac{\omega}{4\bar{P}_3^2}\right) + 6\big[1-4\beta^2+3\beta^4+\omega^2(3+\beta^2) - 4\omega^4\big]\bar{P}_3 \ln\beta \\
& + \big[5-22\beta^2+5\beta^4+9\omega^2(1+\beta^2) - 6\omega^4\big]\bar{P}_3 \Bigg\}\,.
\end{aligned} \tag{2.6}$$

Taking the limit $m_b = 0$ ($\beta \to 0$) we obtain,

$$\begin{aligned}
\alpha_S\Gamma_1(\omega^2) = \Gamma^{(\infty)}\frac{\alpha_S}{2\pi}C_F \Big\{ & 4(1-\omega^2)^2(1+2\omega^2)\Big[\mathrm{Li}_2(1-\omega^2) - \frac{\pi^2}{3} + \frac{1}{2}\ln(1-\omega^2)\ln\omega^2\Big] \\
& -2\omega^2(1+\omega^2)(1-2\omega^2)\ln\omega^2 - (1-\omega^2)^2(4\omega^2+5)\ln(1-\omega^2) + \frac{1}{2}(1-\omega^2)(5+9\omega^2-6\omega^4)\Big\}
\end{aligned} \tag{2.7}$$

The effect of the W-boson Breit-Wigner propagator on the total width can be included as follows [17],

$$\Gamma_t^{BW} = \frac{\gamma\xi}{\pi}\int_0^{(1-\beta)^2} \frac{d\omega^2}{(1-\xi\omega^2)^2+\gamma^2}\Big[\Gamma_0(\omega^2) + \alpha_s\Gamma_1(\omega^2)\Big]\,, \tag{2.8}$$

where ξ and γ are defined in Table 1. The total width for the decay to an on-shell W-boson can be obtained from Eq. (2.8) by imposing the narrow width approximation,

$$\Gamma_t^{NW} = \Big[\Gamma_0(\frac{1}{\xi}) + \alpha_s\Gamma_1(\frac{1}{\xi})\Big]\,. \tag{2.9}$$

As shown in Table 2 the QCD correction results in a relative change in the top quark width,

$$\frac{\alpha_S\Gamma_1}{\Gamma_0} \approx -0.8\alpha_S \tag{2.10}$$

that lowers the leading order result by about 10%.

For our purposes we are interested not so much in the total width but rather in the pattern of gluon radiation associated with top decay. Therefore we need a more differential rate, including both the distributions of the decay products of the W and of the gluon radiation (if present). This will be calculated using a point-by-point subtraction technique that is appropriate for such a calculation [21, 22]. Thus the integrated real and virtual corrections to the decay rate given in ref. [20] are not

[1] We follow closely the presentation in ref. [20]. Eq. (2.6) clarifies the obvious typographical error $S \to 8$ in Eq. (27) of ref. [20]. We thank Andrzej Czarnecki for correspondence on this point. We have slightly modified the form of the expression in Eq. (27) of ref. [20] using dilogarithm identities in order to make the finiteness in the $\beta \to 0$ limit more manifest.

	$m_W = 80.398$ GeV,$m_b = 4.7$ GeV	$m_W = 80.398$ GeV,$m_b = 0$
Γ_0^{BW} [GeV]	1.453518	1.457412
$\Gamma_1^{BW}/\Gamma_0^{BW}$	-0.7878491	-0.7972087
Γ_0^{NW} [GeV]	1.476596	1.480522
$\Gamma_1^{NW}/\Gamma_0^{NW}$	-0.7878090	-0.7971276

Table 2. Values of the LO top width and the NLO correction to the semi-leptonic width, using $G_F = 1.16639 \times 10^{-5}$ and $m_t = 172.5$ GeV. The results are calculated using both the full Breit-Wigner for the width (BW) and using the narrow width approximation (NW). In the former case we take $\Gamma_W = 2.1054$ GeV. The first column represents the complete result for non-zero W and b masses, while in the subsequent column we approximate by setting the b-quark mass to zero.

sufficient for our purposes. Nevertheless the computation of the radiative corrections to the width contains many essential ingredients for our calculation and also provides an important input for our result. Therefore in appendix B we will present details of the calculation of the top decay width, in a language that will allow generalization to the case in which we are interested.

There are further known corrections to the top quark width from electroweak effects [23, 24] and from NNLO QCD [25]. In this paper we do not require these corrections. Since we treat the top quark as strictly on shell, the width of the top quark enters only as a scale factor, to be chosen to ensure that we get the correct branching ratio to the appropriate decay channel. We shall comment more on this issue in Section 6.

3 Amplitudes for top production

Our approach relies on a factorization of the calculation into amplitudes that include the production of a top quark and amplitudes that represent its subsequent decay. This method is restricted to the case of top quarks that are produced exactly on shell, but includes all spin correlations in the decay of the top quark. By factorizing the calculation in this way we have neglected interference effects between radiation in the two stages. Since the characteristic time scale for the production of the top quark is of order $1/m_t$ while the time for the decay is $1/\Gamma_t$, in general radiation in the production and decay stages is separated by a large time and interference effects are expected to be small, of order $\alpha_S \Gamma_t/m_t$ [26–28].

In this section we will illustrate the method using the case of s-channel top production and briefly describe the implementation of the production amplitudes for all top production processes that we consider.

3.1 s-channel single top production

The production of single top by the s-channel process is the simplest to describe. The lowest order process is,

$$\begin{aligned} u(-u) + \bar{d}(-d) \;\to\; & \bar{b}(p_c) + t(p_t) \\ & \hookrightarrow \nu(\nu) + e^+(\bar{e}) + b(p_b) \end{aligned} \tag{3.1}$$

where the momenta of the particles are shown in brackets in an obvious notation. We consider all momenta to be outgoing so that,

$$u + d + p_c + p_t = u + d + p_c + \nu + \bar{e} + p_b = 0. \tag{3.2}$$

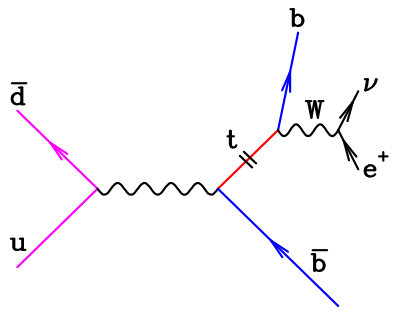

Figure 3. Lowest order diagram for s-channel single top production. The double bar indicates that the top is on mass shell.

Since our method relies on the assumption that the top quark is exactly on shell, and the bottom quarks are also on their mass shells we have that,

$$p_t^2 = m_t^2, \quad p_c^2 = p_b^2 = m_b^2. \tag{3.3}$$

Thus the amplitude for the process in Figure 3 is,

$$M_{\lambda_b\lambda_c} = \delta_{i_d i_u}\delta_{i_b i_c}\frac{g_W^2}{2D_W(s_{ud})}\langle d|\gamma^\rho|u]\ \ \bar{u}_{\lambda_b}(p_b)\gamma^\mu\gamma_L\frac{(\not{p}_t + m_t)}{im_t\Gamma_t}\gamma_\rho\gamma_L v_{\lambda_c}(p_c)\ \ \frac{g_W^2}{2D_W(s_{\nu\bar{e}})}\langle\nu|\gamma^\mu|\bar{e}]\ , \tag{3.4}$$

and $g_W^2 = 4\sqrt{2}m_W^2 G_F$. We have suppressed the colour labels i_d, i_u, i_b and i_c of the d, u, b and $\bar{b}$ quarks on the left-hand side. The matrix γ_L is defined by $\gamma_L = 1 - \gamma_R = \frac{1}{2}(1 - \gamma_5)$, the propagator factor is,

$$D_x(s) = (s - m_x^2) + im_x\Gamma_x\ , \tag{3.5}$$

and $s_{ij} = (i+j)^2$, $s_{ijk} = (i+j+k)^2$ where i, j and k stand for four-momenta. The notations $|i\rangle$ and $|j]$ denote spinor solutions of the massless Dirac equation. A brief summary of our spinor notation is given in Appendix A. Using the identity,

$$\sum_{\lambda_t} u_{\lambda_t}(p_t)\bar{u}_{\lambda_t}(p_t) = \not{p}_t + m_t\ , \tag{3.6}$$

we may write Eq. (3.4) as,

$$M_{\lambda_b\lambda_c} = \sum_{\lambda_t, i_t} D_{\lambda_b\lambda_t}\ \frac{1}{im_t\Gamma_t}\ P_{\lambda_t\lambda_c}\ , \tag{3.7}$$

where the amplitudes representing the production ($P_{\lambda_t\lambda_c}$) and decay ($D_{\lambda_b\lambda_t}$) of the top quark are given by,

$$D_{\lambda_b\lambda_t} = \delta_{i_b i_t}\bar{u}_{\lambda_b}(p_b)\gamma^\mu\gamma_L u_{\lambda_t}(p_t)\ \ \frac{g_W^2}{2D_W(s_{\nu\bar{e}})}\langle\nu|\gamma^\mu|\bar{e}] \equiv \delta_{i_b i_t}\frac{g_W^2}{D_W(s_{\nu\bar{e}})}\bar{u}_{\lambda_b}(p_b)|\nu\rangle[\bar{e}|u_{\lambda_t}(p_t)\ , \tag{3.8}$$

$$\begin{aligned} P_{\lambda_t\lambda_c} &= \delta_{i_t i_c}\delta_{i_d i_u}\frac{g_W^2}{2D_W(s_{ud})}\langle d|\gamma^\rho|u]\ \ \bar{u}_{\lambda_t}(p_t)\gamma_\rho\gamma_L v_{\lambda_c}(p_c) \\ &\equiv \delta_{i_t i_c}\delta_{i_d i_u}\frac{g_W^2}{D_W(s_{ud})}\bar{u}_{\lambda_t}(p_t)|d\rangle[u|v_{\lambda_c}(p_c)\ . \end{aligned} \tag{3.9}$$

These equations have been simplified on the right hand side by using the Fierz-like identity, Eq. (A.5). In order to proceed further we shall use the standard trick [29] of decomposing the massive momenta into the sum of two massless momenta, $p_t^\mu = t^\mu + \alpha_t \eta_t^\mu$ with the constant α_t given by,

$$\alpha_t = \frac{m_t^2}{\langle \eta_t | \not{p}_t | \eta_t]} \, . \tag{3.10}$$

We may write the massive spinors as combinations of massless spinors as follows,

$$u_-(p_t) = (\not{p}_t + m_t)|\eta_t\rangle \frac{1}{\langle t \eta_t \rangle}, \quad u_+(p_t) = (\not{p}_t + m_t)|\eta_t] \frac{1}{[t \eta_t]} \, , \tag{3.11}$$

$$\bar{u}_-(p_b) = [\eta_b|(\not{p}_b + m_b) \frac{1}{[\eta_b b]}, \quad \bar{u}_+(p_b) = \langle \eta_b|(\not{p}_b + m_b) \frac{1}{\langle \eta_b b \rangle} \, , \tag{3.12}$$

$$v_+(p_c) = (\not{p}_c - m_b)|\eta_c\rangle \frac{1}{\langle c \eta_c \rangle}, \quad v_-(p_c) = (\not{p}_c - m_b)|\eta_c] \frac{1}{[c \eta_c]} \, , \tag{3.13}$$

$$\bar{v}_+(p_a) = [\eta_a|(\not{p}_a - m_t) \frac{1}{[\eta_a a]}, \quad \bar{v}_-(p_a) = \langle \eta_a|(\not{p}_a - m_t) \frac{1}{\langle \eta_a a \rangle} \, . \tag{3.14}$$

The momenta p_t and p_a refer to the top and anti-top quark respectively whereas p_b and p_c refer to the bottom and anti-bottom quark. The spin labels of the massless spinors $|\eta_i\rangle, |\eta_i]$ for $i = t, a, b, c$ encode the polarization information of the massive quarks and they are equivalent to helicities only in the massless limit. Stripping the overall colour, coupling and propagator factors,

$$P_{\lambda_t \lambda_c} = \delta_{i_t i_c} \delta_{i_d i_u} \frac{g_W^2}{D_W(s_{ud})} \mathcal{P}_{\lambda_t \lambda_c} \, , \tag{3.15}$$

we can evaluate the production amplitudes in Eq. (3.9) to find,

$$\begin{aligned}
\mathcal{P}_{--} &= -m_b \frac{\langle t\, d \rangle \, [\eta_c \, u]}{[\eta_c \, c]} \to 0 \\
\mathcal{P}_{-+} &= -\langle t\, d \rangle \, [c \, u] \\
\mathcal{P}_{+-} &= -m_b m_t \frac{\langle \eta_t \, d \rangle \, [\eta_c \, u]}{\langle \eta_t \, t \rangle \, [\eta_c \, c]} \to 0 \\
\mathcal{P}_{++} &= -m_t \frac{\langle \eta_t \, d \rangle \, [c \, u]}{\langle \eta_t \, t \rangle} \to m_t \frac{\langle \bar{e} \, d \rangle \, [c \, u]}{\langle t \, \bar{e} \rangle} \, .
\end{aligned} \tag{3.16}$$

The final expressions (in which two of the amplitudes vanish) are valid for the special choices, $\eta_t = \bar{e}, \eta_c = u$. Unless otherwise stated, we shall always simplify our amplitudes with these choices of η_t and η_c.

3.1.1 Virtual corrections to s-channel single top production.

As is apparent from Figure 4 the virtual corrections to the s-channel production are of two types. In the lower row we have the vertex corrections to a timelike vector boson (a) coupling to two massless fermions and (b) coupling to a massive top quark and a massive bottom quark. These corrections are well known and will be considered in more detail in the next section in the context of one-loop corrections to the decay of a top quark. Indeed the identical corrections occur (a) in the hadronic decay of a W boson, and (b) in the one-loop corrections to the semileptonic decay of a top quark. We will therefore defer our discussion of these corrections until later.

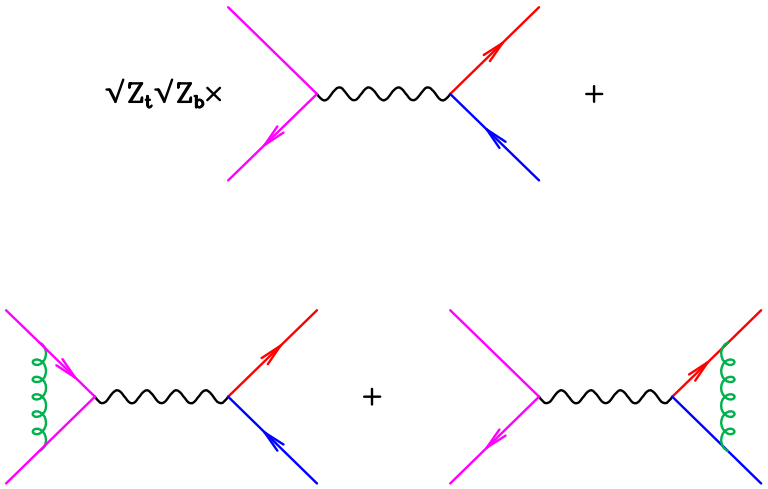

Figure 4. Diagram for s-channel single top production with virtual gluon radiation.

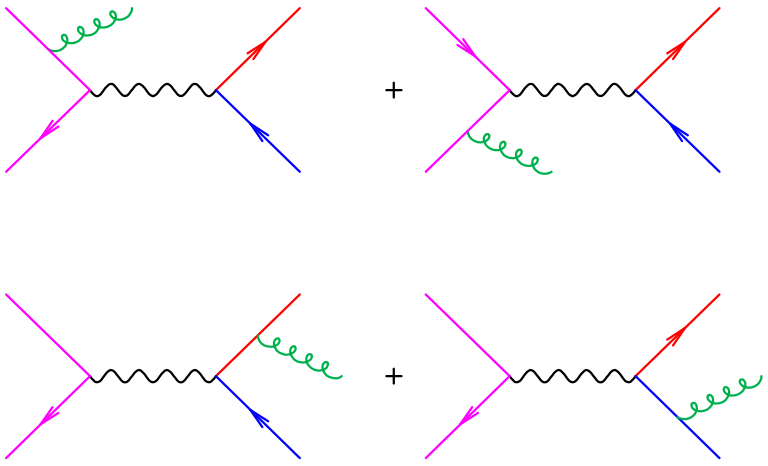

Figure 5. Diagram for s-channel single top production with additional gluon radiation.

3.1.2 Real corrections to s-channel single top production.

Figure 5 shows the diagrams contributing to s-channel single top production in association with an additional radiated gluon. The diagrams in the top row have gluon radiation from the initial state quarks, whereas the diagrams in the bottom row have gluon radiation from the final state quarks. The two rows of diagrams are separately gauge invariant and do not interfere because of colour conservation. In addition to the diagrams in Fig 5 there are also diagrams obtained by crossing the gluon in the top row into the initial state. The diagrams obtained by crossing the gluon in the bottom row into the initial state are not included because they correspond to the t-channel single-top production process and are therefore accounted for elsewhere. We begin by defining the reduced matrix elements for the

real radiation from the initial and final states,

$$P^{(i)}_{\lambda_t\lambda_g\lambda_c} = g_W^2 g_s \left(t^A\right)_{i_d i_u} D_W(s_{udg}) \mathcal{P}^{(i)}_{\lambda_t\lambda_g\lambda_c}\,, \tag{3.17}$$

$$P^{(f)}_{\lambda_t\lambda_g\lambda_c} = g_W^2 g_s \left(t^A\right)_{i_t i_c} D_W(s_{ud}) \mathcal{P}^{(f)}_{\lambda_t\lambda_g\lambda_c}\,, \tag{3.18}$$

where the colour matrices t^A are normalized such that $t^A t^B = \delta^{AB}$. The spin labels $\lambda_t, \lambda_h, \lambda_c$ encode the polarization state of the top quark, gluon and bottom anti-quark respectively. After a simple calculation we find for radiation from the initial state,

$$\begin{aligned}
\mathcal{P}^{(i)}_{---} &= 0 \\
\mathcal{P}^{(i)}_{--+} &= \frac{\langle t|d+g|u]\,[c\,u]}{[g\,u]\,[g\,d]} \\
\mathcal{P}^{(i)}_{+--} &= 0 \\
\mathcal{P}^{(i)}_{+-+} &= -\frac{m_t\,\langle \bar{e}|d+g|u]\,[c\,u]}{\langle t\,\bar{e}\rangle\,[g\,u]\,[g\,d]} \\
\mathcal{P}^{(i)}_{-+-} &= \frac{m_b\,\langle t\,d\rangle\,[g\,u]}{\langle g\,u\rangle\,[c\,u]} \\
\mathcal{P}^{(i)}_{-++} &= \frac{\langle d|u+g|c]\,\langle t\,d\rangle}{\langle g\,u\rangle\,\langle g\,d\rangle} \\
\mathcal{P}^{(i)}_{++-} &= -\frac{m_t m_b\,\langle \bar{e}\,d\rangle\,[g\,u]}{\langle t\,\bar{e}\rangle\,\langle g\,u\rangle\,[c\,u]} \\
\mathcal{P}^{(i)}_{+++} &= -\frac{m_t\,\langle d|u+g|c]\,\langle \bar{e}\,d\rangle}{\langle t\,\bar{e}\rangle\,\langle g\,u\rangle\,\langle g\,d\rangle}\,.
\end{aligned} \tag{3.19}$$

The results for radiation from the final-state quarks are,

$$\begin{aligned}
\mathcal{P}^{(f)}_{---} &= 0 \\
\mathcal{P}^{(f)}_{--+} &= -\frac{\langle t\,d\rangle\,[c\,u]}{[g\,d]}\left(\frac{\langle g|p_t|d]}{\langle g|p_t|g]} - \frac{\langle g|p_c|d]}{\langle g|p_c|g]}\right) + \frac{\langle t\,g\rangle\,\langle g\,d\rangle\,[c\,u]}{\langle g|p_t|g]} \\
\mathcal{P}^{(f)}_{+--} &= 0 \\
\mathcal{P}^{(f)}_{+-+} &= \frac{m_t\,\langle \bar{e}\,d\rangle\,[c\,u]}{\langle t\,\bar{e}\rangle\,[g\,d]}\left(\frac{\langle g|p_t|d]}{\langle g|p_t|g]} - \frac{\langle g|p_c|d]}{\langle g|p_c|g]}\right) + \frac{m_t\,\langle g\,\bar{e}\rangle\,\langle g\,d\rangle\,[c\,u]}{\langle t\,\bar{e}\rangle\,\langle g|p_t|g]} \\
\mathcal{P}^{(f)}_{-+-} &= \frac{m_b\,\langle t\,d\rangle\,[g\,u]^2}{[c\,u]\,\langle g|p_c|g]} \\
\mathcal{P}^{(f)}_{-++} &= \frac{\langle t\,d\rangle\,[c\,u]}{\langle g\,u\rangle}\left(\frac{\langle u|p_t|g]}{\langle g|p_t|g]} - \frac{\langle u|p_c|g]}{\langle g|p_c|g]}\right) + \frac{\langle t\,d\rangle\,[c\,g]\,[g\,u]}{\langle g|p_c|g]} \\
\mathcal{P}^{(f)}_{++-} &= -\frac{m_t m_b\,\langle \bar{e}\,d\rangle\,[g\,u]^2}{\langle t\,\bar{e}\rangle\,[c\,u]\,\langle g|p_c|g]} \\
\mathcal{P}^{(f)}_{+++} &= -\frac{m_t\,\langle \bar{e}\,d\rangle\,[c\,u]}{\langle t\,\bar{e}\rangle\,\langle g\,u\rangle}\left(\frac{\langle u|p_t|g]}{\langle g|p_t|g]} - \frac{\langle u|p_c|g]}{\langle g|p_c|g]}\right) - \frac{m_t\,\langle \bar{e}\,d\rangle\,[c\,g]\,[g\,u]}{\langle t\,\bar{e}\rangle\,\langle g|p_c|g]}\,.
\end{aligned} \tag{3.20}$$

3.2 Top pair production

In our current treatment of top pair production we have followed the procedure outlined above and expressed the complete amplitude as a product of the amplitude for $t\bar{t}$ production times the amplitude for the decay of the top quark and the anti-quark. In addition we have coded the analytic results for

the one-loop amplitudes for top pair production given in the paper of Badger et al., ref. [30]. These amplitudes are expressed simply in terms of spinor products. Our previous treatment of the one-loop amplitudes [3] was based on the work of Körner et al. [31] in which the results are expressed in terms of more complicated spinor strings. We note that the two calculations are in complete numerical agreement. We find that using the new expressions of Ref. [30] in MCFM improves the speed of the calculation of the virtual corrections by a factor of three.

3.3 t-channel single top production

For the t-channel single top process we use the four-flavour scheme in which the lowest order process is,

$$q + g \to q' + \bar{b} + t(\to \nu e^+ b) \,, \tag{3.21}$$

as indicated in the top row of Figure 2. The next-to-leading order corrections to this process, without including the top decay products (i.e. $qg \to q'\bar{b}t$), were presented in Refs. [11, 12]. In this paper we re-use the amplitudes computed for that calculation but extend them to incorporate the top quark decay in a fashion similar to the approach presented for the other two cases above. A slight difference is that the virtual amplitudes used in Ref. [11, 12] had already been simplified by making a specific choice for the vectors that are used to decompose the massive top quark momentum, η_t. In that case the standard decay amplitudes that are presented in the following section cannot be used. Rather than repeat the calculation of the relevant amplitudes with the canonical choice of this vector used throughout the rest of this paper, we have simply used expressions for the Born-level decay amplitudes (see Eq. (4.4) in the next section) that are appropriate for this alternative choice of η_t.

4 Amplitudes for top decay

In this section we list the various decay amplitudes that are used in the calculations presented in this paper. Except where otherwise noted, we make the choices $\eta_t = \bar{e}, \eta_b = \nu$, with the choice of η_t required in order to match the production amplitudes.

4.1 Top decay at Born level

The Born decay amplitudes for the process

$$t(p_t) \to b(p_b) + \nu(\nu) + e^+(\bar{e}) \tag{4.1}$$

can be easily evaluated from the expression given in Eq. (3.8). In order to report the results using spinor products it is useful to define the massless vectors, $t \cdot t = b \cdot b = 0$, using the auxiliary vectors, η_b, η_t,

$$\begin{aligned} t^\mu &= p_t^\mu - \frac{m_t^2}{2p_t.\eta_t}\eta_t^\mu \,, \\ b^\mu &= p_b^\mu - \frac{m_b^2}{2p_b.\eta_b}\eta_b^\mu \,. \end{aligned} \tag{4.2}$$

Separating out the colour, coupling and propagator factors,

$$D_{\lambda_b\lambda_t} = \delta_{i_b i_t}\, \frac{g_W^2}{D_W(s_{\nu\bar{e}})}\, \mathcal{D}_{\lambda_b\lambda_t} \,, \tag{4.3}$$

we find,

$$\begin{aligned}
\mathcal{D}_{--} &= \langle b\nu\rangle[\bar{e}t] \\
\mathcal{D}_{-+} &= m_t\langle b\nu\rangle\frac{[\bar{e}\eta_t]}{[t\eta_t]} \to 0 \\
\mathcal{D}_{+-} &= m_b\frac{\langle\eta_b\nu\rangle}{\langle\eta_b b\rangle}[\bar{e}t] \to 0 \\
\mathcal{D}_{++} &= m_b m_t\frac{\langle\eta_b\nu\rangle}{\langle\eta_b b\rangle}\frac{[\bar{e}\eta_t]}{[t\eta_t]} \to 0\,.
\end{aligned} \tag{4.4}$$

Making the choices $\eta_t = \bar{e}$ (as in the production amplitudes) and $\eta_b = \nu$, all but the amplitude $\mathcal{D}_{--}$ vanish.

As noted above, for the particular case of virtual and real radiation corrections to the t-channel production process the amplitudes have already been simplified using $\eta_t = g$, the momentum of the gluon in the initial state. One can read off the appropriate decay amplitudes from Eq. (4.4) by making the choices $\eta_t = g, \eta_b = \nu$. We see that in this case the amplitude $\mathcal{D}_{-+}$ does not vanish.

The amplitudes for the related charge-conjugate process,

$$\bar{t}(p_a) \to \bar{b}(p_c) + e^-(e) + \bar{\nu}(\bar{\nu})\,, \tag{4.5}$$

can be obtained from the above amplitudes by symmetry. Denoting the colour-stripped amplitudes for this process by $\overline{\mathcal{D}}_{\lambda_a\lambda_c}$ and introducing the operator $\mathcal{C}$ defined by,

$$\mathcal{C}: \qquad t \to a\,, \quad b \to c\,, \quad \nu \to \bar{\nu}\,, \quad \bar{e} \to e\,, \quad \langle i\,j\rangle \leftrightarrow [i\,j]\,, \tag{4.6}$$

then we have,

$$\overline{\mathcal{D}}_{\lambda_a\lambda_c} = -\mathcal{C}\left[\mathcal{D}_{-\lambda_b\,-\lambda_t}\right]\,. \tag{4.7}$$

Note that the massless vectors a and c that appear in the expressions for the amplitudes are related to the massive four-momenta of the top and bottom quarks, p_a and p_c, by the transformed equivalents of Eq. (4.2),

$$a^\mu = p_a^\mu - \frac{m_t^2}{2p_a.\eta_a}\eta_a^\mu\,, \qquad c^\mu = p_c^\mu - \frac{m_b^2}{2p_c.\eta_c}\eta_c^\mu\,, \tag{4.8}$$

with the choices $\eta_a = e$ and $\eta_c = \bar{\nu}$.

4.2 Virtual corrections to top decay

We now discuss top quark decay with virtual gluon radiation from the t, b line as shown in the top row of Figure 6. We give the results for the special choices, $\eta_t = \bar{e}, \eta_b = \nu$ for the one loop corrections to the decay, $\mathcal{D}^V_{\lambda_b\lambda_t}$. The labels λ_b and λ_t denote the spin state of the bottom and top quark respectively. In the massless limit they would correspond to helicities. The general result for the renormalized one-loop form factor in the case $m_t \neq 0, m_b \neq 0$ is,

$$\mathcal{F}_\mu(p_b, p_t) = \frac{g_W}{\sqrt{2}}\bar{u}(p_b)\Gamma_\mu(p_b, p_t)u(p_t)\,, \tag{4.9}$$

where $\Gamma_\mu(p_b, p_t)$ is decomposed as,

$$\begin{aligned}
\Gamma^\mu(p_b, p_t) &= \gamma^\mu\gamma_L + g^2\,C_F c_\Gamma\left(\frac{\mu^2}{m_t^2}\right)^\epsilon \times \\
&\left[\,C_0^L\gamma^\mu\gamma_L + C_0^R\gamma^\mu\gamma_R + C_1^R\frac{p_b^\mu}{m_t}\gamma_R + C_1^L\frac{p_b^\mu}{m_t}\gamma_L + C_2^R\frac{p_W^\mu}{m_t}\gamma_R + C_2^L\frac{p_W^\mu}{m_t}\gamma_L\right] + O(\epsilon)
\end{aligned} \tag{4.10}$$

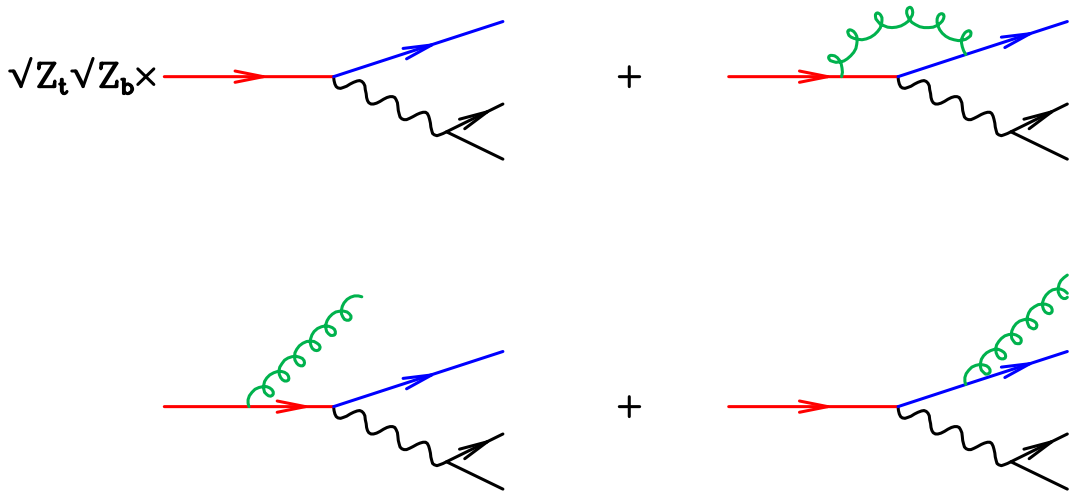

Figure 6. Diagrams for gluon radiation from the t, b-line in top decay. Z_b and Z_t denote the wave function renormalization constants for the external fermion lines. The expression for the $Z_q, (q = b, t)$ is given in the appendix, Eq. (B.7).

The factor c_Γ is the standard prefactor that appears in dimensionally regulated one-loop calculations,

$$c_\Gamma = \frac{1}{(4\pi)^{2-\epsilon}} \frac{\Gamma(1+\epsilon)\Gamma^2(1-\epsilon)}{\Gamma(1-2\epsilon)} = \frac{1}{(4\pi)^{2-\epsilon}} \frac{1}{\Gamma(1-\epsilon)} + O(\epsilon^3) \,. \tag{4.11}$$

If we ignore the masses of the decay products of the W-boson, the $C_2^{L/R}$ terms will not contribute to physical amplitudes. They will be dropped in the following. The results for the remaining coefficients are given in Eq. (B.6) of Appendix B.2. The amplitudes C_0^R, C_1^L and C_1^R are finite in the limit $\epsilon \to 0$. Removing the common overall factor,

$$D^V_{\lambda_b \lambda_t} = \delta_{i_b i_t} \frac{g_W^2 g_s^2 c_\Gamma C_F}{D_W(s_{\nu\bar{e}})} \left(\frac{\mu^2}{m_t^2}\right)^\epsilon \mathcal{D}^V_{\lambda_b \lambda_t} \,, \tag{4.12}$$

we have that,

$$\begin{aligned}
\mathcal{D}^V_{--} &= \left\{ C_0^L \langle b\,\nu\rangle [\bar{e}\,t] + \frac{C_1^R}{2} \frac{\langle b\,\nu\rangle \langle \bar{e}\,b\rangle [\bar{e}\,b]}{\langle \bar{e}\,t\rangle} + m_t m_b C_0^R \frac{\langle \bar{e}\,\nu\rangle [\nu\,\bar{e}]}{\langle \bar{e}\,t\rangle [\nu\,b]} + \frac{m_b}{m_t} \frac{C_1^L}{2} \frac{\langle b\,\nu\rangle [\nu\,t] [\bar{e}\,b]}{[\nu\,b]} \right\} \\
\mathcal{D}^V_{-+} &= \left\{ m_b C_0^R \frac{\langle \nu\,t\rangle [\nu\,\bar{e}]}{[\nu\,b]} - \frac{C_1^R}{2m_t} \langle \nu\,b\rangle \langle b\,t\rangle [\bar{e}\,b] + m_b \frac{C_1^L}{2} \frac{\langle \nu\,b\rangle [\nu\,\bar{e}] [\bar{e}\,b]}{[\nu\,b] [\bar{e}\,t]} \right\} \\
\mathcal{D}^V_{+-} &= \left\{ m_t C_0^R \frac{\langle \nu\,\bar{e}\rangle [\bar{e}\,b]}{\langle \bar{e}\,t\rangle} - \frac{C_1^L}{2m_t} \langle \nu\,b\rangle [\bar{e}\,b] [b\,t] + m_b \frac{C_1^R}{2} \frac{\langle \nu\,\bar{e}\rangle [\bar{e}\,b]}{\langle \bar{e}\,t\rangle} \right\} \\
\mathcal{D}^V_{++} &= \left\{ C_0^R \langle t\,\nu\rangle [\bar{e}\,b] + \frac{C_1^L}{2} \frac{\langle b\,\nu\rangle [\bar{e}\,b]^2}{[\bar{e}\,t]} + \frac{C_1^R}{2} \frac{m_b}{m_t} \langle t\,\nu\rangle [\bar{e}\,b] \right\} .
\end{aligned} \tag{4.13}$$

Because of the vanishing results in Eq. (4.4), $\mathcal{D}_{+\lambda_t} = 0$, for our particular choice of auxiliary vectors, η_t, η_b the one-loop results for $\mathcal{D}^V_{+-}, \mathcal{D}^V_{++}$ will not be needed.

The virtual amplitudes for the decay of an anti-top quark are related to those for the decay of a top quark in the same manner as for the lowest order amplitudes. Namely,

$$\overline{\mathcal{D}}^V_{\lambda_a\lambda_c} = -\mathcal{C}\left[\mathcal{D}^V_{-\lambda_b\,-\lambda_t}\right] \,, \tag{4.14}$$

where the operation $\mathcal{C}$ is defined in Eq. (4.6).

4.3 Top decay with gluon radiation

We now discuss top quark decay with gluon radiation from the t, b line as shown in the bottom row of Figure 6. In order to report the results using spinor products it is useful to define the massless vectors, $t \cdot t = b \cdot b = 0$, as in Eq. (4.2), using the auxiliary vectors, $\bar{e}, \nu$,

$$t^\mu = p_t^\mu - \frac{m_t^2}{2p_t.\bar{e}}\bar{e}^\mu \,, \qquad b^\mu = p_b^\mu - \frac{m_b^2}{2p_b.\nu}\nu^\mu \,. \tag{4.15}$$

We further define the colour-stripped decay amplitudes through the relation,

$$D^R_{\lambda_b\lambda_g\lambda_t} = g_s\mu^\epsilon (t^A)_{i_b i_t}\,\frac{g_W^2}{D_W(s_{\nu\bar{e}})}\,\mathcal{D}^R_{\lambda_b\lambda_g\lambda_t} \,, \tag{4.16}$$

where the colour matrices t^A are normalized such that $t^A t^B = \delta^{AB}$. The explicit expressions for the decay amplitudes are,

$$\begin{aligned}
\mathcal{D}^R_{---} &= \frac{\langle b\,\nu\rangle\,[t\,\bar{e}]}{[b\,g]}\left(\frac{\langle g|p_b|b]}{\langle g|p_b|g]} - \frac{\langle g|p_t|b]}{\langle g|p_t|g]}\right) + \frac{\langle b\,g\rangle\,\langle g\,\nu\rangle\,[t\,\bar{e}]}{\langle g|p_b|g]} \,,\\
\mathcal{D}^R_{-+-} &= \frac{\langle b\,\nu\rangle\,[t\,\bar{e}]}{\langle g\,b\rangle}\left(\frac{[g|p_b|b\rangle}{[g|p_b|g\rangle} - \frac{[g|p_t|b\rangle}{[g|p_t|g\rangle}\right) + \frac{\langle b\,\nu\rangle\,[g\,t]\,[g\,\bar{e}]}{[g|p_t|g\rangle} \,,\\
\mathcal{D}^R_{+--} &= \frac{m_b\,\langle\nu\,g\rangle^2\,[\bar{e}\,t]}{\langle\nu\,b\rangle\,\langle g|p_b|g]} \,,\\
\mathcal{D}^R_{++-} &= 0 \,,\\
\mathcal{D}^R_{--+} &= 0 \,,\\
\mathcal{D}^R_{-++} &= \frac{m_t\,\langle\nu\,b\rangle\,[\bar{e}\,g]^2}{[\bar{e}\,t]\,\langle g|p_t|g]} \,,\\
\mathcal{D}^R_{+-+} &= 0 \,,\\
\mathcal{D}^R_{+++} &= 0 \,.
\end{aligned} \tag{4.17}$$

As expected the soft gluon singularities are all contained in the eikonal terms for $\mathcal{D}^R_{---}$ and $\mathcal{D}^R_{-+-}$. These can be simplified using the Schouten identity, Eq.(A.6), to remove the unphysical singularity. For example, the amplitude $\mathcal{D}_{---}$ contains the singular term,

$$\frac{1}{[b\,g]}\left(\frac{\langle g|p_b|b]}{\langle g|p_b|g]} - \frac{\langle g|p_t|b]}{\langle g|p_t|g]}\right) = \frac{\langle g|\not{p}_b\not{p}_t|g\rangle}{\langle g|p_b|g]\,\langle g|p_t|g]} \,. \tag{4.18}$$

Squaring the part of the full decay amplitude that contains the eikonal factor we obtain the standard expression,

$$\left|D^R_{---}\right|^2 = g_s^2\mu^{2\epsilon}Tr(t^A t^A)\left|\frac{\langle g|\not{p}_b\not{p}_t|g\rangle}{\langle g|p_b|g]\,\langle g|p_t|g]}\right|^2 = \frac{1}{2}g_s^2\mu^{2\epsilon}C_F\times\left[-\frac{m_b^2}{(p_b.g)^2} + \frac{2p_t.p_b}{p_b.g\,p_t.g} - \frac{m_t^2}{(p_b.g)^2}\right]|D_{--}|^2 \,, \tag{4.19}$$

and an equal result from the other gluon polarization, D^R_{-+-}.

This eikonal form is the basis for the counter-term that we use to subtract the singularities resulting from radiation of a soft gluon in the top quark decay. We make use of the factorization,

$$g_s^2 C_F \mu^{2\epsilon} \sum_{\lambda_b,\lambda_g,\lambda_t} |\mathcal{D}_{\lambda_b\lambda_g\lambda_t}(p_t, p_W, p_b, p_g)|^2 \to \sum_{\lambda_b,\lambda_t} |\mathcal{D}_{\lambda_b\lambda_t}|^2(p_t, \tilde{p}_W, \tilde{p}_b) \times S(p_t.p_g, p_b.p_g, m_t^2, m_b^2, p_W^2) \,, \tag{4.20}$$

where the lowest order matrix element $\mathcal{D}$ is evaluated for momenta $\tilde{p}_W$, $\tilde{p}_b$ of the W-boson and b-quark, as described in more detail in Section 5. In practice, we shall not use the complete eikonal factor as a counterterm, but rather a simpler expression that differs from the above by finite terms. Using

$$(p_t - p_b - g)^2 = p_W^2 \,, \tag{4.21}$$

and dropping non-singular terms we obtain,

$$S(p_t.p_g, p_b.p_g, m_t^2, m_b^2, p_W^2) = g_s^2(\mu^2)^\epsilon C_F \times \Big[-\frac{m_b^2}{(p_b.g)^2} + \frac{m_t^2 + m_b^2 - p_W^2}{p_b.g\, p_t.g} - \frac{m_t^2}{(p_b.g)^2} \Big] \,. \tag{4.22}$$

The amplitudes for the emission of a gluon from the $\bar{t}$-$\bar{b}$ line in anti-top quark decay are related to the amplitudes presented above, in a similar manner to the lowest order case. We have,

$$\overline{\mathcal{D}}^R_{\lambda_a\lambda_g\lambda_c} = \mathcal{C}\left[\mathcal{D}^R_{-\lambda_b\,-\lambda_g\,-\lambda_t}\right] \,, \tag{4.23}$$

where the operation $\mathcal{C}$ is defined in Eq. (4.6). We note that, since these amplitudes contain an additional gluon, this relation is different by an overall sign from those presented in Eqs. (4.7) and (4.14).

4.4 Top decay with virtual gluon radiation from the decay products of the W

If the W boson decays hadronically,

$$t(p_t) \to b(p_b) + q(q) + \bar{q}(\bar{q}) \,, \tag{4.24}$$

then we should also include the next-to-leading order corrections to that decay process, as depicted in Figure 7. The result for the virtual corrections to the decay of a vector boson into a pair of massless fermions is well known [32]. We can write the form factor as,

$$\mathcal{F}_\mu(\bar{q}, q) = \frac{g_W}{\sqrt{2}} \bar{u}(\bar{q}) \Gamma_\mu(\bar{q}, q) u(q) \,, \qquad q^2 = \bar{q}^2 = 0 \,, \tag{4.25}$$

where the expansion is very simple compared to the general case (c.f. Eq. (4.10)),

$$\Gamma^\mu(\bar{q}, q) = \gamma^\mu \gamma_L \Big[1 + g^2\, C_F c_\Gamma C^L \Big] + O(\epsilon) \,. \tag{4.26}$$

Stripping overall colour-factors as usual,

$$D^{V_W}_{\lambda_b\lambda_t} = \delta_{i_b i_t} \frac{g_W^2 g_s^2 c_\Gamma C_F}{D_W(s_{q\bar{q}})} \Big(\frac{\mu^2}{-s_{q\bar{q}} - i\varepsilon} \Big)^\epsilon \mathcal{D}^{V_W}_{\lambda_b\lambda_t} \tag{4.27}$$

all of the amplitudes vanish except one,

$$\mathcal{D}^{V_W}_{--} = C^L \langle bq \rangle [\bar{q}t] \,. \tag{4.28}$$

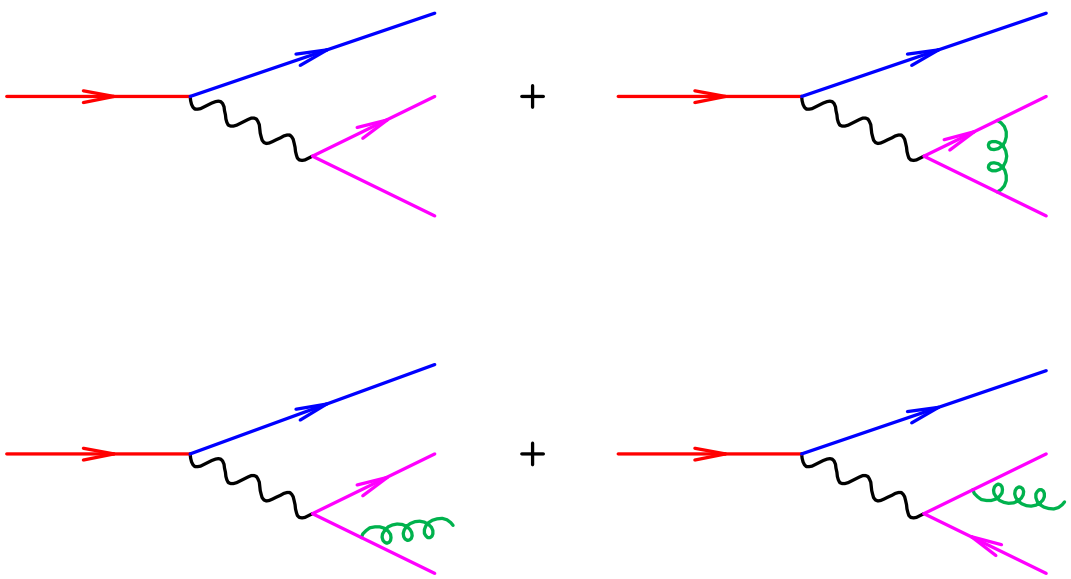

Figure 7. Radiative corrections due to the interaction of the decay products of the W in top decay. The upper line shows the virtual corrections and the lower line the real corrections.

Note that, for the labelling of momenta indicated in Eq. (4.24), the massless momenta t and b are defined by choosing $\eta_t = \bar{q}$ and $\eta_b = q$ in Eq. (4.2). In the four-dimensional helicity scheme the coefficient C^L takes the familiar form,

$$C^L = -\frac{2}{\epsilon^2} - \frac{3}{\epsilon} - 7 \,. \tag{4.29}$$

The amplitudes for the related charge-conjugate process,

$$\bar{t}(p_a) \to \bar{b}(p_c) + q(q) + \bar{q}(\bar{q}) \,, \tag{4.30}$$

can be obtained by a symmetry operation that differs from that in Eq. (4.6) only by a relabelling of momenta. We have,

$$\overline{\mathcal{D}}^{V_W}_{\lambda_a \lambda_c} = -\mathcal{C}_W \left[\mathcal{D}^{V_W}_{-\lambda_b\, -\lambda_t} \right] \,. \tag{4.31}$$

where $\mathcal{C}_W$ is defined by,

$$\mathcal{C}_W : \qquad t \to a \,, \quad b \to c \,, \quad q \to \bar{q} \,, \quad \bar{q} \to q \,, \quad \langle i\, j \rangle \leftrightarrow [i\, j] \,, \tag{4.32}$$

The massless momenta a and c are defined by the choices $\eta_a = q$ and $\eta_c = \bar{q}$ in Eq. (4.8).

4.5 Top decay with real gluon radiation from the decay products of the W

The diagrams for real radiation of a gluon in the W decay are shown in the bottom row of Figure 7. After removing overall factors,

$$D^{R_W}_{\lambda_b \lambda_g \lambda_t} = g_s \mu^\epsilon (t^A)_{i_q \bar{i}_{\bar{q}}} \frac{g_W^2}{D_W(s_{q\bar{q}g})} \mathcal{D}^{R_W}_{\lambda_b \lambda_g \lambda_t} \,, \tag{4.33}$$

a simple calculation yields the amplitudes,

$$\begin{aligned}
\mathcal{D}^{R_W}_{---} &= -\frac{[\bar{q}\,t]\,\langle b|p_W|\bar{q}]}{[q\,g]\,[\bar{q}\,g]}\,, \\
\mathcal{D}^{R_W}_{-+-} &= -\frac{\langle q\,b\rangle\,\langle q|p_W|t]}{\langle q\,g\rangle\,\langle \bar{q}\,g\rangle}\,, \\
\mathcal{D}^{R_W}_{+--} &= m_b\frac{\langle q\,g\rangle\,[\bar{q}\,t]}{\langle q\,b\rangle\,[q\,g]}\,, \\
\mathcal{D}^{R_W}_{++-} &= 0\,, \\
\mathcal{D}^{R_W}_{--+} &= 0\,, \\
\mathcal{D}^{R_W}_{-++} &= -m_t\frac{\langle q\,b\rangle\,[\bar{q}\,g]}{\langle \bar{q}\,g\rangle\,[\bar{q}\,t]}\,, \\
\mathcal{D}^{R_W}_{+-+} &= 0\,, \\
\mathcal{D}^{R_W}_{+++} &= 0\,,
\end{aligned} \tag{4.34}$$

where $p_W = p_q + p_{\bar{q}} + p_g$. The counterterm in this case is the standard Catani-Seymour dipole associated with final-final radiation from massless partons [22].

The equivalent amplitudes for the anti-top quark decay process are given by,

$$\overline{\mathcal{D}}^{R_W}_{\lambda_a\lambda_g\lambda_c} = \mathcal{C}_W\left[\mathcal{D}^{R_W}_{-\lambda_b\,-\lambda_g\,-\lambda_t}\right]\,, \tag{4.35}$$

where the operation $\mathcal{C}_W$ is defined in Eq. (4.32). Once again this relation has the opposite sign from that in Eq. (4.31).

5 Counter-term for real radiation

In this section we describe the implementation of the counter-term that is used to cancel the soft singularity resulting from real radiation from the t-b line in the decay of the top quark. The counter-term has already been introduced in Eq. (4.20), which makes clear that the lowest order matrix element is evaluated at momenta $\tilde{p}_W$ and $\tilde{p}_b$ of the W boson and bottom quark respectively. These momenta are related to those for which the real radiation matrix element is evaluated (p_W, p_b, p_g) as follows.

The transformed momenta $\tilde{p}_W$ and $\tilde{p}_b$ are generated by a Lorentz boost along the direction of the W in the top rest frame, following the method of ref. [2] (Section IV). The transformation is generalized slightly in order to incorporate the effect of a non-zero bottom quark mass. Thus we still have $\tilde{p}^\mu_W = \Lambda^\mu{}_\nu\, p^\nu_W$ with,

$$\begin{aligned}
\Lambda^{\mu\nu} &= g_{\mu\nu} + \frac{\sinh(x)}{\sqrt{(p_t\cdot p_W)^2 - p_W^2 p_t^2}}\left(p_t^\mu p_W^\nu - p_W^\mu p_t^\nu\right) \\
&+ \frac{\cosh(x)-1}{(p_t\cdot p_W)^2 - p_W^2 p_t^2}\left(p_t\cdot p_W\,(p_t^\mu p_W^\nu + p_W^\mu p_t^\nu) - p_W^2\,p_t^\mu p_t^\nu - p_t^2\,p_W^\mu p_W^\nu\right)
\end{aligned} \tag{5.1}$$

but $\tilde{p}_b$ is now constrained by $\tilde{p}_b^2 = (p_t - \tilde{p}_W)^2 = m_b^2$. This constraint determines the coefficients that appear in the transformation,

$$\begin{aligned}
\sinh(x) &= \frac{1}{2\,p_t^2 p_W^2}\left[-\sqrt{\lambda(p_t^2,p_W^2,p_b^2)}\,p_t\cdot p_W + (p_t^2+p_W^2-p_b^2)\sqrt{(p_t\cdot p_W)^2 - p_W^2 p_t^2}\,\right]\,, \\
\cosh(x) &= \frac{1}{2\,p_t^2 p_W^2}\left[+(p_t^2+p_W^2-p_b^2)p_t\cdot p_W - \sqrt{\lambda(p_t^2,p_W^2,p_b^2)}\,\sqrt{(p_t\cdot p_W)^2 - p_W^2 p_t^2}\,\right]\,.
\end{aligned} \tag{5.2}$$

This Lorentz transformation is also used to determine the modified momenta of the W decay products.

With the subtraction fully specified, we now turn to the issue of performing the integration of this counter-term analytically in order that the poles can be extracted and cancelled against those appearing in the virtual calculation. From Eq. (B.14) we may write the phase space for the decay of an on-shell top quark as

$$\begin{aligned} d\Phi^{(3)}(p_t; p_W, p_b, p_g) &= d\Phi^{(2)}(p_t; p_W, p_b) \times [dg(p_t, p_W, z)] \\ &\equiv d\Phi^{(2)}(p_t; \tilde{p}_W, \tilde{p}_b) \times [dg(p_t, \tilde{p}_W, z)] \,. \end{aligned} \tag{5.3}$$

The equivalence in Eq. (5.3) follows from Eq. (B.1) in the appendix because $d^{n-1}\omega_w = d^{n-1}\omega_{\tilde{w}}$ since p_W and $\tilde{p}_W$ are related by a boost.

The counter-term may now be integrated in exactly the same manner as the real radiation matrix elements that enter the calculation of the total width, as detailed in Appendix B. The integrated counter-term corresponds to the sum of the integrals S_1, S_2 and S_3, expressions for which are given in Eqs. (B.23), (B.24) and (B.25). We thus arrive at the final expression for the integrated counter-term,

$$\begin{aligned} &\int [dg(p_t, \tilde{p}_W, z)]\, S(p_t.p_g, p_b.p_g, m_t^2, m_b^2, p_W^2) = S_1 + S_2 + S_3 = \\ &2g^2 c_\Gamma C_F \left(\frac{\mu^2}{m_t^2}\right)^\epsilon \left\{ \left[\frac{2}{\epsilon} - 4\ln\left(\frac{4\bar{P}_3^2}{\omega\beta}\right)\right]\left(1 - \frac{\bar{P}_0}{\bar{P}_3}\bar{Y}_p\right) + 4 + \frac{2}{\bar{P}_3}\Big((1-\omega^2)\bar{Y}_p + (1-\beta^2)\bar{Y}_w\Big) \right. \\ &\left. + \frac{\bar{P}_0}{\bar{P}_3}\Big[2\bar{Y}_p - 6\bar{Y}_p^2 + 4\bar{Y}_w \ln(\beta) - 6\,\mathrm{Li}_2\left(1 - \frac{\bar{P}_-}{\bar{P}_+}\right) - 2\,\mathrm{Li}_2\left(1-\bar{P}_+\right) + 2\,\mathrm{Li}_2\left(1-\bar{P}_-\right)\Big] \right\} . \end{aligned} \tag{5.4}$$

6 Consistent treatment of top quark decay in perturbation theory

Since we are everywhere treating the top quark as on shell, the full cross section integrated over the decay products of the top will be given by the production cross section multiplied by the branching fraction to the chosen decay channel. This statement should hold at all orders in perturbation theory. For example, we can write the differential NLO cross section for single top production followed by semi-leptonic decay schematically as,

$$\sigma^{NLO}(pp \to t(\to \nu e^+ b) + X) = (\sigma_0 + \alpha_S \sigma_1) \times \frac{d\Gamma_0^{(l)} + \alpha_S d\Gamma_1^{(l)}}{\Gamma_0 + \alpha_S \Gamma_1} \,, \tag{6.1}$$

where σ_0, $\Gamma_0^{(l)}$, Γ_0 are the lowest order contributions to the production rate, semileptonic decay width $\Gamma(t \to \nu e^+ b)$, and total top width and $\alpha_S\sigma_1$, $\alpha_S\Gamma_1^{(l)}$ and $\alpha_S\Gamma_1$ the corresponding NLO corrections. The total top width is given by the sum of the partial widths to the various decay channels,

$$\Gamma_t = \sum_{i,j} \Gamma(t \to f_i \bar{f}_j b + X) \,, \tag{6.2}$$

which factorizes in the narrow width approximation for the W-boson to,

$$\Gamma_t \to \Gamma(t \to bW + X) \times \sum_{i,j} \frac{\Gamma(W \to f_i \bar{f}_j)}{\Gamma_W} \equiv \Gamma(t \to bW + X) \,. \tag{6.3}$$

The quantity $\Gamma(t \to bW + X)$ has the perturbative expansion, $\Gamma(t \to bW + X) = \Gamma_0 + \alpha_S\Gamma_1$, where Γ_0, Γ_1 are as given in Eqs. (2.2), (2.6). This is the expression for the total width used in the denominator of Eq. (6.1).

In order to include the effect of radiation in the decay of the top quark properly, we must be careful to ensure that we perform the perturbative expansion in the strong coupling in a consistent manner. As written in Eq. (6.1) the NLO calculation includes a contribution of relative order α_S^2 corresponding to corrections in both production and decay stages simultaneously. We follow the treatment in ref. [14] and simply expand Eq.(6.1) in α_S, discarding terms of order α_S^2 or higher,

$$\sigma^{NLO} = \sigma_0 \times \frac{d\Gamma_0^{(l)}}{\Gamma_0} + \sigma_0 \times \frac{\alpha_S d\Gamma_1^{(l)}}{\Gamma_0} + \alpha_S\sigma_1 \times \frac{d\Gamma_0^{(l)}}{\Gamma_0} - \alpha_S\sigma_0 \times \frac{d\Gamma_0^{(l)}}{\Gamma_0}\frac{\Gamma_1}{\Gamma_0} \,. \tag{6.4}$$

Performing the full integration over the final state, i.e. making the substitutions $d\Gamma_0^{(l)} \to \Gamma_0^{(l)}$ and $d\Gamma_1^{(l)} \to \Gamma_1^{(l)}$, we recover the NLO cross section for corrections in production only,

$$\begin{aligned}\sigma^{NLO} &= (\sigma_0 + \alpha_S\sigma_1) \times Br(W \to \nu e^+) + \alpha_S\sigma_0 Br(W \to \nu e^+)\left[\frac{\Gamma_1^{(l)}}{\Gamma_0^{(l)}} - \frac{\Gamma_1}{\Gamma_0}\right] \\ &\equiv (\sigma_0 + \alpha_S\sigma_1) \times Br(W \to \nu e^+)\end{aligned} \tag{6.5}$$

where the equality follows, for example in the narrow width approximation, because,

$$\frac{\Gamma_1^{(l)}}{\Gamma_0^{(l)}} = \frac{\Gamma_1(t \to bW + X)Br(W \to \nu e^+)}{\Gamma_0(t \to bW + X)Br(W \to \nu e^+)} \,. \tag{6.6}$$

We note that while Eq. (6.5) is a desirable outcome, it is only true in the case that all degrees of freedom associated with the decay are completely integrated out. In the presence of experimental cuts, for instance on the leptons or b-quarks present in the decay, the two calculations (i.e. with and without radiation in decay), can predict different cross sections. The above discussion pertains to the case of NLO corrections to the production and leptonic decay of a single top quark. For top pair production, with both top quarks decaying leptonically, the last term that appears in Eq. (6.4) appears once for each quark so that this correction factor is doubled.

We note that since the top quark is produced exactly on-shell, the value of the top quark width is important only to ensure that we obtain the correct branching ratio when including the decay. This can clearly be achieved by using Γ_0 as shown in Eq. (6.4). This is therefore the value of the width used in our code.

The argument given above also holds, *mutatis mutandis*, for hadronic instead of leptonic decays of the W-boson.

7 Phenomenology

7.1 Input parameters

The results presented in this paper are obtained with the latest version of the MCFM code (v6.2). The electroweak parameters that we regard as inputs are,

$$M_W = 80.398 \text{ GeV} \,, \quad \Gamma_W = 2.1054 \text{ GeV} \,, \tag{7.1}$$

$$G_F = 1.16639 \times 10^{-5} \text{ GeV}^{-2} \,. \tag{7.2}$$

The top and bottom quarks have the pole masses,

$$m_t = 172.5 \text{ GeV} \,, \quad m_b = 4.7 \text{ GeV} \,. \tag{7.3}$$

Treatment of W-boson and b-quark	σ_{LO} [fb]	σ_{NLO} (prod.) [fb]	σ_{NLO} (prod.+decay) [fb]
Narrow width, $m_b = 0$	30.98(2)	48.84(3)	48.82(3)
Narrow width, $m_b = 4.7$ GeV	30.78(2)	48.61(3)	48.60(3)
Breit-Wigner, $m_b = 4.7$ GeV	30.77(2)	48.61(3)	48.59(3)

Table 3. Cross sections in femtobarns for the s-channel single top process, computed with various levels of sophistication. No cuts have been applied to the final state. The numerical integration errors are shown in brackets.

For the parton distribution functions (pdfs) we use the sets of Martin, Stirling, Thorne and Watt [33]. For the calculation of the LO results presented here we employ the corresponding LO pdf fit, with 1-loop running of the strong coupling and $\alpha_s(M_Z) = 0.13939$. Similarly, at NLO we use the NLO pdf fit, with $\alpha_s(M_Z) = 0.12018$ and 2-loop running.

In our calculations of the top pair and s-channel single top processes we set the factorization and renormalization scales equal to the top quark mass. For the t-channel process we employ two scales, one for evaluating contributions associated with the light quark line (μ_l) and the other for the heavy quark line (μ_h). We set $\mu_l = m_t/2$ and $\mu_h = m_t/4$, as advocated in Ref. [12].

7.2 s-channel single top at the Tevatron

In order to illustrate some of the features of our calculation, we begin by considering the s-channel single top process. Although the thrust of this paper is the inclusion of the top quark decay allowing realistic experimental cuts to be applied to the top decay products, it it instructive to first consider the case in which no cuts are applied.

The predicted cross section for the process $p\bar{p} \to t(\to \nu e^+ b)\bar{b}$ at the Tevatron, computed at various levels of sophistication, is shown in Table 3. In this table we present results of performing the calculation at LO, at NLO including radiation in production only, and at NLO including radiation in both production and decay. Moreover, we consider three different kinematic approximations: setting $m_b = 0$ and using the narrow-width approximation for the W-boson (equivalent to the approach in Ref. [2]), using $m_b = 4.7$ GeV but still using the narrow-width approach, and finally using $m_b = 4.7$ GeV and implementing the full Breit-Wigner form of the W propagator. We first observe that, by construction, the two columns of calculated NLO cross sections are in perfect agreement, thanks to the presence of the last term in Eq. (6.4). Moreover, the slight adjustment to the width of the W-boson when using the Breit-Wigner rather than the narrow-width approximation, as indicated in Table 2, ensures that the final two rows of Table 3 are also in excellent agreement. Finally, we observe that the effect of including the b-mass in this process is very small, resulting in a decreases in the cross-section by approximately 0.5%. We note that this effect is not the result of including the mass of the b-quark in the top quark decay but is instead due to the treatment of the $\bar{b}$ quark.

We now perform the same analysis using a realistic set of experimental cuts. In particular we use the cuts employed in a recent search for the Higgs boson using the $WH(\to b\bar{b}$ associated production channel, for which s-channel single top production is an irreducible background [34]. All jets (both light and heavy flavour) are clustered according to the anti-k_T algorithm with a distance parameter $D = 0.7$. We require that the algorithm finds at least two jets that satisfy,

$$p_T(\text{jet}) > 20 \text{ GeV} , \qquad y(\text{jet}) < 2 . \tag{7.4}$$

and the charged lepton acceptance is defined by,

$$p_T(\text{lepton}) > 20 \text{ GeV} , \qquad y(\text{lepton}) < 1 . \tag{7.5}$$

Treatment of W-boson and b-quark	σ_{LO} [fb]	σ_{NLO} (prod.) [fb]	σ_{NLO} (prod.+decay) [fb]
Narrow width, $m_b = 0$	12.14(2)	19.96(2)	20.03(2)
Narrow width, $m_b = 4.7$ GeV	12.12(2)	19.96(2)	20.01(2)
Breit-Wigner, $m_b = 4.7$ GeV	12.08(2)	19.88(2)	19.95(2)

Table 4. Cross sections in femtobarns for the s-channel single top process, computed with various levels of sophistication. The cuts appropriate for the Higgs search, as described in the text, have been applied.

In addition we require that there is at least 20 GeV of missing transverse momentum. Our results for the process $p\bar{p} \to t(\to \nu e^+ b)\bar{b}$ under this set of cuts are shown in Table 4. As anticipated, the application of cuts results in a small difference between the two columns of NLO results. We find that the NLO cross section including radiation in production and decay stages is approximately 0.3% higher than the result for radiation in production only. For similar reasons, the cuts also induce a slight reduction in the cross section (by less than 0.5%) when working with the full Breit-Wigner propagator rather than in the narrow width approximation. We also see that the effect of including the b-mass is negligible, due to the requirement that at least two jets are reconstructed with transverse momenta that are relatively large compared to the b-quark mass.

7.3 t-channel single top at the LHC

The production of single top quarks via the t-channel process is the dominant production mode at the LHC. The final state is hard to distinguish from top pair production and a variety of QCD backgrounds such as the production of a W boson in association with jets. In order to distinguish single top events from the main background processes, a recent CMS analysis [35] relies on accurate theoretical predictions for two observables.

The first is the rapidity of the light jet that is present in the event. Since at LO this light jet is produced by the t-channel emission of a W boson from an initial quark, it is found primarily in the forward direction, in contrast to the centrally-produced light jets from background processes. The second observable, $\cos\theta^\star$ is computed by performing a boost to the rest frame of the reconstructed top quark and then defining $\theta^\star$ as the angle between the charged lepton and the light jet in that frame. For both these observables it is interesting to investigate to what extent the distributions are modified by higher order corrections to both the production and decay processes.

For the study presented here we have adopted the cuts from Ref. [35]. Light and heavy-flavour jets are clustered according to the anti-k_T algorithm with a distance parameter $D = 0.5$ and only satisfy a fairly loose set of cuts,

$$p_T(\text{jet}) > 30 \text{ GeV} , \qquad y(\text{jet}) < 5 . \tag{7.6}$$

The cuts on the charged lepton are,

$$p_T(\text{lepton}) > 20 \text{ GeV} , \qquad y(\text{lepton}) < 2.1 , \tag{7.7}$$

and no requirement is made on the missing transverse momentum. Following the CMS analysis, we demand that exactly two jets are present after jet clustering: the appropriately-charged bottom jet and a light (non-tagged) jet. We reconstruct the top quark by combining the leptonically decaying W boson (reconstructed perfectly, by assumption) with the b-jet. If the invariant mass of the W-b-light-jet system is closer to m_t than the invariant mass of the W-b system then the radiation is assumed to occur in the decay and the event is dropped.

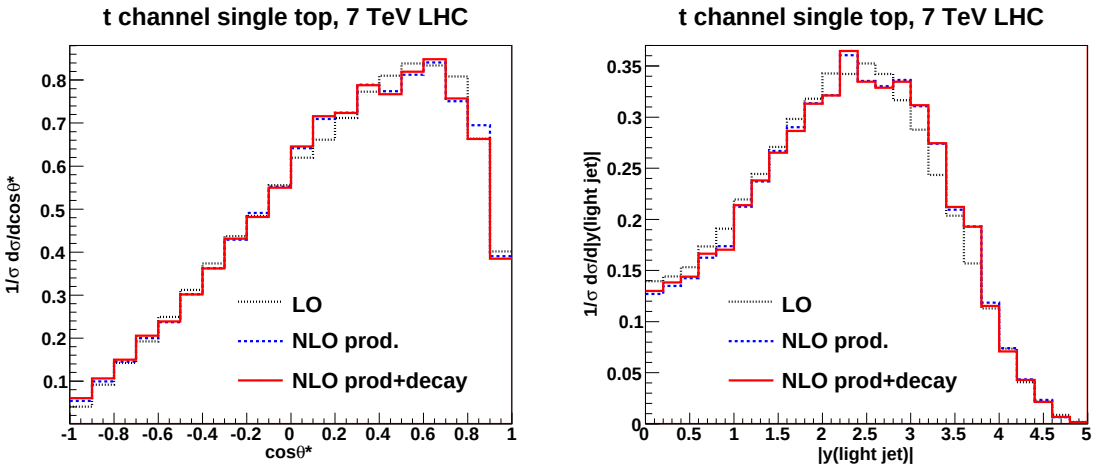

Figure 8. Distributions of $\cos\theta^*$ (defined in the text) and $|y_{\rm light}$ at the 7 TeV LHC, computed using the set of cuts described in the text and adapted from Ref. [35].

Our results are shown in Figure 8. We observe that the effect of the NLO corrections in the production is a slight change in the shape of both distributions. However, the effect of additionally including the radiation in the decay is not significant.

7.4 Top pair phenomenology

The phenomenology of top pair production is very rich in comparison with the single top processes due to the much higher production cross section. We therefore perform a more detailed study of top pair production in this section.

7.4.1 Top production at the LHC

We first provide predictions for some basic kinematic distributions that have recently been analyzed by the CMS collaboration [36]. The cuts employed in our study are the ones presented in that analysis. Both light and heavy-flavour partons are clustered according to the anti-k_T algorithm with a distance parameter $D = 0.5$ and the resulting jets must satisfy the acceptance cuts,

$$p_T(\text{jet}) > 30 \text{ GeV} , \qquad y(\text{jet}) < 2.4 . \tag{7.8}$$

We require that two b-jets are found by the algorithm, out of a total of at least two jets (for the dilepton case, with the top and anti-top decay leptonically) and at least four jets (in the lepton+jets case, with one top decaying hadronically). The cuts on the charged lepton depend on the decay channel:

$$\begin{aligned} \text{dilepton}: \quad & p_T(\text{lepton}) > 20 \text{ GeV} , \qquad y(\text{lepton}) < 2.4 , \\ \text{lepton+jets}: \quad & p_T(\text{lepton}) > 30 \text{ GeV} , \qquad y(\text{lepton}) < 2.1 , \end{aligned} \tag{7.9}$$

but no requirement is made on the missing transverse momentum.

We will also present distributions for the W bosons, top and anti-top quarks that are reconstructed according to the following algorithm. For simplicity we assume that a leptonically decaying W is perfectly reconstructed. For a hadronic W decay we consider as candidates all pairs of light jets and,

if there are three light jets, also the system of all three together (to account for radiation in the decay). The system whose invariant mass is closest to m_W is assigned as the hadronic W decay. For the top and anti-top quarks, we consider both the system consisting of the W and the appropriate bottom quark, and the system that also contains the remaining light jet (if it was not already assigned to the W decay). The combination of assignments that results in invariant masses closest to m_t for both top and anti-top quarks is considered the proper solution. We note that, since we produce both top and anti-top quarks on-shell, this reconstruction is often perfect. However, in the case that initial state radiation in the production stage is merged with a bottom quark in the final state, one of the top quark masses may be reconstructed far from its mass shell. We have not tried to remove such configurations in the results presented here, although the code is flexible enough to pursue such approaches.

In Figure 9 we present a selection of observables for the dilepton process. Focusing first on the leptonic observables we see that the NLO corrections have a considerable impact on the shape of the p_T distribution of the charged leptons but that their rapidity distribution is left unchanged. Moreover, the effect of including NLO corrections in the decay of the top quark is negligible. Turning to the observables obtained after reconstruction of the top and anti-top quark momenta, we see that the rapidity distribution of the top quarks is not affected by the QCD corrections. The shape of the transverse momentum distribution of a single top quark does receive substantial corrections at large $p_T \gtrsim 250$ GeV. In addition, the two NLO curves also differ: the prediction when including QCD radiation in the top decay lies between the LO and NLO (production only) curves.

For the lepton+jets channel we consider the process $pp \to t(\to e^+\nu b)\bar{t}(\to e^-\bar{\nu}\bar{b}) + X$, i.e. we consider the leptonic decay of the top quark and the hadronic decay of the anti-top quark. In Figure 10 we show the invariant mass spectrum of the W^+ and W^- bosons produced in this process. We note that for the W^+ boson we have made the simplification that the neutrino 4-momentum is known, while the W^- boson is reconstructed according to the algorithm above. We see that, at LO, the predicted distribution for W^- is identical to W^+, since there is no ambiguity in identifying the jets (we assume that the b-jets are perfectly tagged). However, at NLO the additional radiation – either before or after the top quark decay – may be mistakenly assigned to the W^- boson, leading to the substantial change in shape of the distribution. In addition there is a significant difference between the two NLO predictions, with radiation in the decay leading to a bigger enhancement in the region $m_{jj} < M_W$.

In Figure 11 we show the invariant mass of the top, anti-top system in both the dilepton and lepton+jets channels. This distribution is important for New Physics searches and, in both cases, although we observe important NLO effects at high $m_{t\bar{t}}$, this is purely due to the treatment of NLO effects in the production stage and not in the decay.

Finally in Figure 12 we present the distributions of two additional observables for the dilepton channel - the transverse momentum of the positively charged lepton, $p_T(\ell^+)$ and the invariant mass of the ℓ^+ and b-quark system, $m_{\ell^+,b}$. As first pointed out in Ref. [14], in the context of the LHC operating at 10 TeV, the latter distribution is particularly interesting since it exhibits differences between the NLO predictions with and without including QCD corrections in the decay (in the region just below the LO threshold at m_t). Here we simply note that the same pattern is observed at 7 TeV, under typical analysis cuts used for the 2011 run, as was noted in Ref. [14]. In passing we also remark that our predictions are in complete agreement with those of Ref. [14] once the appropriate differences in input parameters are accounted for.

7.4.2 The top quark forward-backward asymmetry at the Tevatron

A feature of top quark production at the Tevatron that has recently received much attention is the top quark forward-backward asymmetry [37–40]. The predicted asymmetry is only non-zero at NLO

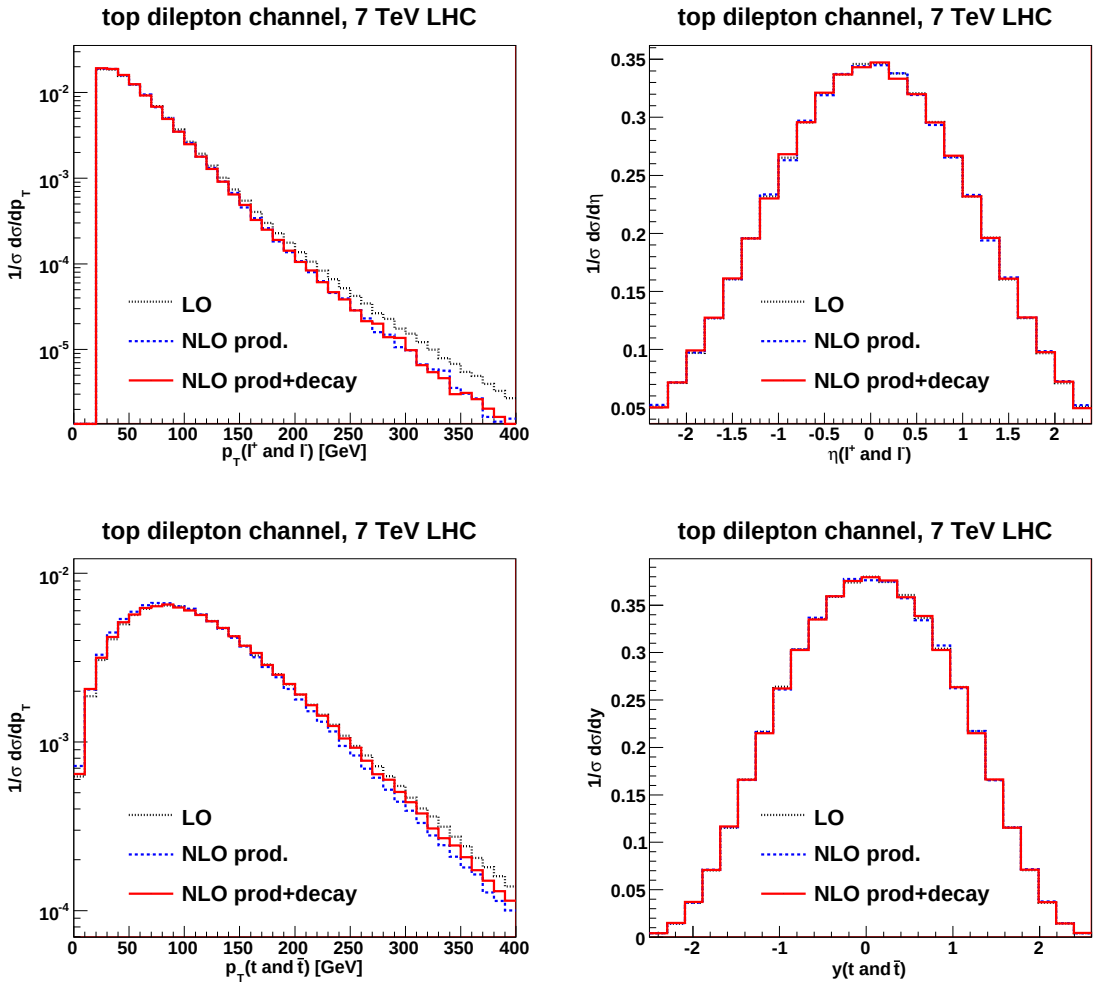

Figure 9. Predictions for various observables in the top pair dilepton channel at 7 TeV LHC, calculated at LO (black), NLO in production (blue) and NLO in production and decay (red). The observables are: the p_T (top left) and rapidity (top right) of the charged leptons and the p_t and rapidity of the reconstructed top and anti-top quarks. In each case, a single event enters the histograms twice, once each for the particle (ℓ or t) and anti-particle ($\bar{\ell}$ or $\bar{t}$).

and beyond and, as an example of the utility of our calculation, in this section we provide a prediction for the parton-level asymmetry within the fiducial coverage of the CDF detector.

To that end, we focus on the lepton+jets channel and adapt an analysis approach based on that presented in a recent CDF note [40]. Partons are clustered using the anti-k_T algorithm with distance parameter $D = 0.4$ and we require that at least four jets are found that satisfy,

$$p_T(\text{jet}) > 20 \text{ GeV} , \qquad y(\text{jet}) < 2 . \tag{7.10}$$

In addition, we demand that both the b and $\bar{b}$ quarks are identified within these jets, with those jets detected in the restricted rapidity range, $y(b - \text{jet}) < 1$. For the leptonic top decay we require,

$$p_T(\text{lepton}) > 20 \text{ GeV} , \qquad y(\text{lepton}) < 1.5 , \tag{7.11}$$

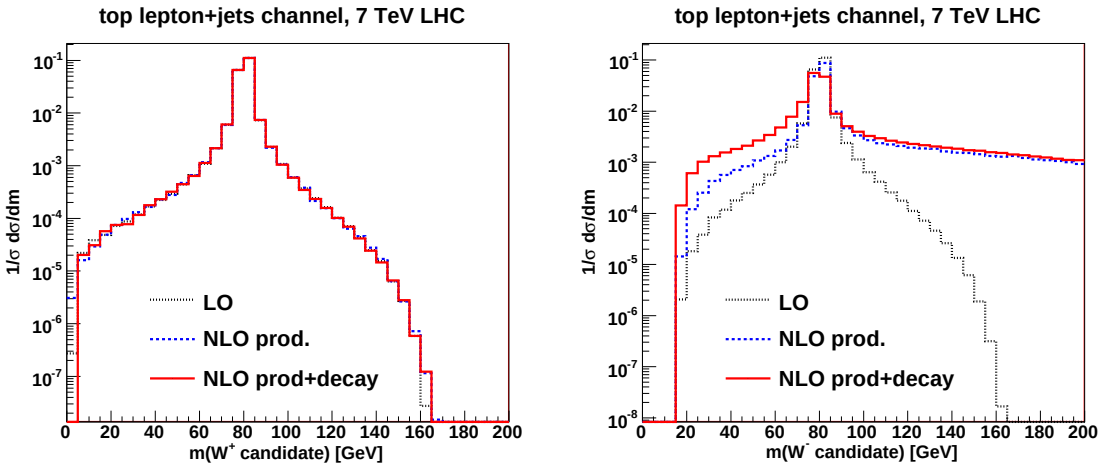

Figure 10. Distribution of the W-boson candidate invariant masses in the lepton+jets channel at the 7 TeV LHC. The top quark decays leptonically, so the W^+ candidate (left) is perfectly reconstructed, while the anti-top quark decays hadronically leading to ambiguity in the reconstruction of the W^--boson at NLO (right).

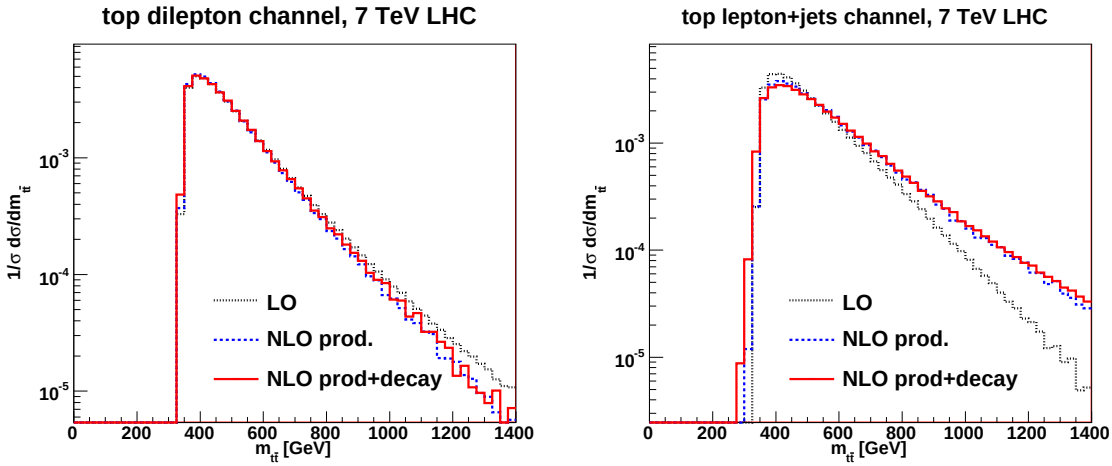

Figure 11. Distribution of the invariant mass of the top, anti-top quark system at the 7 TeV LHC, for the dilepton channel (left) and the lepton+jets channel (right).

and at least 20 GeV of missing transverse momentum (from the neutrino). The top and anti-top quarks are reconstructed using the same procedure as in the LHC lepton+jets analysis described above.

As for all the previous results, our predictions are based on the choice of scale $\mu_R = \mu_F = m_t$. Ordinarily a NLO prediction is relatively insensitive to the choice of scale but, in this case, since the asymmetry is absent in the LO prediction our results depend rather strongly on the choice of scale. For this reason we also consider variations of this scale by a factor of two about this central choice, i.e. in the range $(m_t/2, 2m_t)$, and take the variation in the prediction as an estimate of the theoretical

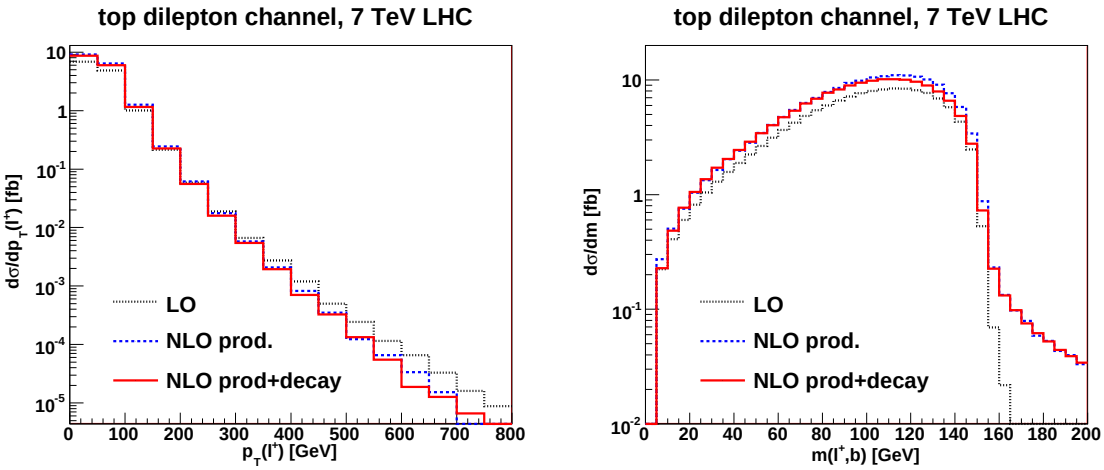

Figure 12. Distribution of the transverse momentum of the positively charged lepton, ℓ^+ (left) and the invariant mass of the ℓ^+ and b-quark, $m_{\ell^+ b}$ (right) in the top pair dilepton channel at the 7 TeV LHC.

uncertainty due to uncalculated higher orders. For each calculation we compute the asymmetry,

$$A_{\rm FB} = \frac{\sigma_{\rm NLO}\left(\Delta y > 0\right) - \sigma_{\rm NLO}\left(\Delta y < 0\right)}{\sigma_{\rm NLO}\left(\Delta y > 0\right) + \sigma_{\rm NLO}\left(\Delta y < 0\right)}\,, \tag{7.12}$$

where the rapidity difference is defined by $\Delta y = y_t - y_{\bar{t}}$. Our results are presented in Table 5 where, for the sake of comparison, we also include predictions for the asymmetry in the absence of any cuts on the decay products of the top quarks. In addition to computing $A_{\rm FB}$ inclusively, we also present predictions broken down into contributions over various rapidity difference ranges. As can be seen from Table 5 the theoretical uncertainties permit excursions from the central value of as much as 60%. Had we used the leading order prediction in the denominator of Eq. (7.12) the estimated theoretical uncertainties would have been smaller. As such, the use of the NLO result in the denominator is a conservative choice. We observe that the asymmetry expected in the fiducial range is smaller than that predicted in the full rapidity range, but grows with Δy. The predictions for the two NLO calculations, with and without NLO effects in the decay, do not differ greatly. Since the component of the calculation that includes radiation in the decay contains no asymmetry one might expect the computations that include these effects to result in a smaller value of $A_{\rm FB}$. In contrast, we find that in the region $\Delta y > 0.5$ the cross section under the experimental cuts is lower in the presence of radiation in the decay, so that the denominator in Eq. (7.12) is reduced and the predicted $A_{\rm FB}$ higher.

Our results are compared to the CDF results reported in Ref. [40] in Figure 13.[2] The inclusive calculation, with no cuts, can be compared in a straightforward manner with the "parton-level" corrected results that are presented in the CDF note. In contrast, when the experimental cuts are applied, the comparison must be interpreted with considerable caution. Our analysis differs somewhat from that used by CDF, notably in the treatment of the top quark reconstruction, but most importantly the CDF data is simply background-subtracted and not corrected back to the parton level. In that case, our theoretical predictions should be interfaced with a parton shower in order that a full detector

[2] The theoretical predictions in Ref. [40] include a 26% correction to the asymmetry because of electroweak contributions. These corrections will not be included in our results.

Rapidity range	$A_{\rm FB}^{\rm no\ cuts}$(NLO)	$A_{\rm FB}^{\rm cuts}$(NLO production)	$A_{\rm FB}^{\rm cuts}$(NLO prod + decay)
inclusive	$0.065^{+0.028}_{-0.014}$	$0.044^{+0.017}_{-0.010}$	$0.045^{+0.021}_{-0.011}$
$0 < \|\Delta y\| < 0.5$	$0.036^{+0.020}_{-0.003}$	$0.017^{+0.005}_{-0.005}$	$0.015^{+0.009}_{-0.004}$
$0.5 < \|\Delta y\| < 1$	$0.062^{+0.013}_{-0.028}$	$0.052^{+0.019}_{-0.012}$	$0.053^{+0.025}_{-0.011}$
$1 < \|\Delta y\| < 1.5$	$0.101^{+0.060}_{-0.006}$	$0.086^{+0.035}_{-0.017}$	$0.092^{+0.039}_{-0.021}$
$\|\Delta y\| > 1.5$	$0.193^{+0.058}_{-0.036}$	$0.142^{+0.059}_{-0.034}$	$0.149^{+0.062}_{-0.036}$

Table 5. Predictions for the top forward-backward asymmetry in the lepton+jets channel at the Tevatron, computed without applying any experimental cuts ($A_{\rm FB}^{\rm no\ cuts}$) and also when using the cuts described in the text ($A_{\rm FB}^{\rm cuts}$). The uncertainties are obtained by varying the scale in the range $(m_t/2, 2m_t)$.

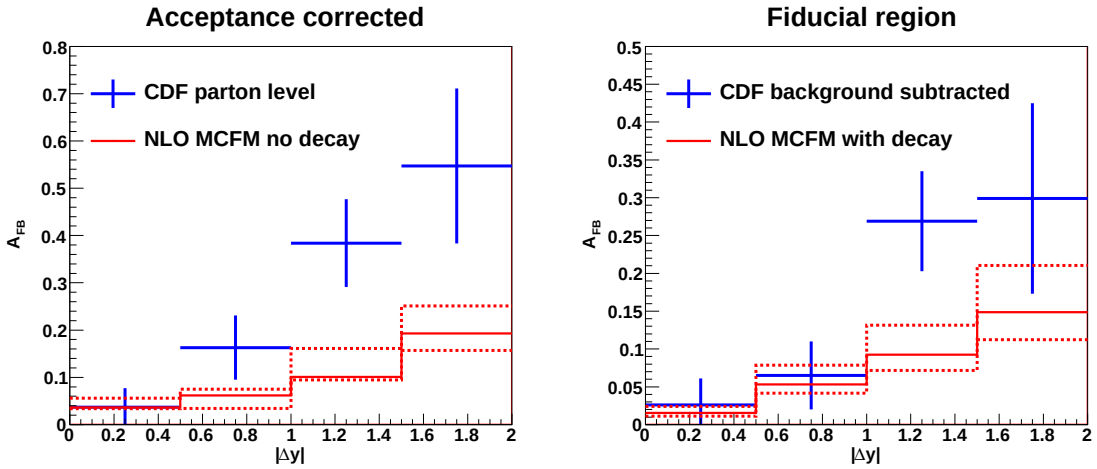

Figure 13. The top quark forward-backward asymmetry, $A_{\rm FB}$, at the Tevatron, after acceptance for corrections (left) and in the measured fiducial region as detailed in the text (right). Data are taken from CDF [40] (Tables IX and XVI) and the MCFM predictions are for inclusive $t\bar{t}$ production (left) and for the differential rate including radiation in both production and decay (right). The central prediction is shown as a solid line and the dashed lines represent an estimate of the theoretical uncertainty.

simulation be performed before making a definitive comparison. Nevertheless, our results can be taken as a guide to the level of uncertainty expected in current predictions of the asymmetry as a function of Δy.

We conclude with predictions for an observable that does not depend on reconstructing the top quark kinematics and that would not be expected to receive significant corrections due to the addition of a parton shower. This observable is the asymmetry observed in the charge-weighted rapidity distribution of the lepton (i.e. $q_\ell \eta_\ell$). The lepton inherits the asymmetry of the top quark and its properties should be predicted more robustly by our calculation. Using the same procedure for assigning the uncertainty as before we find,

$$A_{\rm FB}^{\rm lepton}(\text{NLO production}) = 0.021^{+0.006}_{-0.005}\,, \qquad A_{\rm FB}^{\rm lepton}(\text{NLO prod+decay}) = 0.020^{+0.010}_{-0.003}\,. \tag{7.13}$$

These predictions should be compared with the most recent CDF result [40],

$$A_{\rm FB}^{\rm lepton}({\rm CDF}) = 0.065 \pm 0.020\,. \tag{7.14}$$

8 Conclusions

In this paper we have described in detail the implementation of single top and top pair processes in the parton-level integrator MCFM. We have presented an amplitude-level treatment that allows the inclusion of the decay at NLO for all processes involving top quarks. We have currently implemented this scheme in MCFM for three processes, top-pair production, s-channel single top production, and t-channel single top production.

Our treatment of top-pair production has been rewritten to use this method and to incorporate a faster treatment of the one-loop amplitudes. By retaining the mass for the b quark we can work in a four-flavour scheme for the t-channel single top process. In this scheme the bottom quark does not appear in the initial state, but the production cross section depends logarithmically on the mass of the b-quark. The four-flavour t-channel single top production, implemented using this method and presented in this paper is new.

The features we have described are complete as of MCFM v6.2. MCFM therefore provides the most sophisticated possible NLO treatment of these top production processes within the context of the top pole approximation. With these features we can assess the importance of NLO radiative effects in production and decay, the effect of the b quark mass, and the effect of an off-shell W-boson. For the distributions that we have examined, these effects turn out to be quite small.

We look forward to confronting this implementation of NLO theory with data.

Acknowledgments We gratefully acknowledge useful conversations with Simon Badger and Markus Schulze. This research is supported by the US DOE under contract DE-AC02-06CH11357.

A Spinor notation

Our spinor notation is quite standard in the QCD literature, (for a review see refs. [41, 42]). The function $u_\pm(k_i)$ is a massless Weyl spinor of momentum k_i and positive or negative chirality. In terms of these solutions of the Dirac equation, the spinor products are defined by,

$$\langle i\,j\rangle \;=\; \langle i^-|j^+\rangle = \bar{u}_-(k_i)u_+(k_j)\,, \tag{A.1}$$

$$[i\,j] \;=\; \langle i^+|j^-\rangle = \bar{u}_+(k_i)u_-(k_j)\,. \tag{A.2}$$

We use the convention $[i\,j] = {\rm sgn}(k_i^0 k_j^0)\,\langle j\,i\rangle^*$, so that,

$$\langle i\,j\rangle\,[j\,i] = 2k_i\cdot k_j \equiv s_{ij}\,. \tag{A.3}$$

and

$$\langle j\,i\rangle = -\,\langle i\,j\rangle\,, \qquad\qquad [j\,i] = -\,[i\,j]\,. \tag{A.4}$$

For massless spinors we have the following generalization of the Fierz identity,

$$\langle a|\gamma^\mu|b]\;\gamma_\mu = 2\,(|a\rangle[b| + |b]\langle a|)\,. \tag{A.5}$$

Another useful identity is the Schouten identity,

$$\begin{aligned} \langle a\,b\rangle\,\langle c\,d\rangle &= \langle a\,d\rangle\,\langle c\,b\rangle + \langle a\,c\rangle\,\langle b\,d\rangle\ , \\ [a\,b]\,[c\,d] &= [a\,d]\,[c\,b] + [a\,c]\,[b\,d]\ . \end{aligned} \tag{A.6}$$

We further define,

$$\langle a|\not{p}|b] \equiv \langle a|p|b] \to \langle a\,p\rangle\,[p\,b] \text{ for massless } p, \tag{A.7}$$

where the decomposition into a pair of spinor products is only valid for a massless momentum p.

B Calculation of the total width for top decay

Our calculation retains the NLO corrections to the fully differential top decay rate. This requires the inclusion of the correlations with the decay products of the W-boson as well as the effects of extra gluon radiation if present. The calculation of the total width that we detail here sums over the polarizations of the W-boson and integrates over the momentum emitted gluon. Although this is not a new result, the total width is one of the ingredients in our calculation. In addition, the calculation of the one-loop contribution to the differential rate is almost identical to the calculation of the one-loop contribution to the total width and our integration over the real radiation counterterm closely parallels the integration over the real radiation given below. Our treatment of the corrections to the width follows, and in places supplements, the nice discussion given in ref. [20].

B.1 Phase space for tree graph top decay

In the rest frame of the top it is straightforward to obtain the two particle phase space for the decay $t \to W + b$,

$$\begin{aligned} d\Phi^{(2)}(p_t; p_W, p_b) &= \frac{d^n p_b}{(2\pi)^{n-1}} \frac{d^n p_W}{(2\pi)^{n-1}} (2\pi)^n\, \delta^n(p_t - p_W - p_b)\, \delta(p_b^2 - m_b^2)\, \delta(p_W^2 - m_W^2) \\ &= \frac{(4\pi)^{2\epsilon}}{32\pi^2} \frac{1}{(m_t^2)^\epsilon} \left[\lambda(1, \omega^2, \beta^2)\right]^{\frac{1}{2}-\epsilon} d^{n-2}\Omega_w\ , \end{aligned} \tag{B.1}$$

where $\omega = m_W/m_t$, $\beta = m_b/m_t$ and $\lambda(x, y, z)$ is defined in Table 1. The matrix element squared for this process, summed over spins, is,

$$\mathcal{M}_\mu \mathcal{M}_\nu^* \left(-g^{\mu\nu} + \frac{p_W^\mu p_W^\nu}{m_W^2} \right) = \frac{2 G_F m_t^4}{\sqrt{2}} f\,, \tag{B.2}$$

with f also defined in Table 1. Using the fact that,

$$\int d^{n-2}\Omega_w = (4\pi)^{1-\epsilon} \frac{\Gamma(1-\epsilon)}{\Gamma(2-2\epsilon)}\ , \tag{B.3}$$

taking the limit $\epsilon \to 0$ and including the flux factor $(2m_t)^{-1}$, we recover the result for the lowest order width quoted in Eq. (2.2).

B.2 Virtual corrections to top decay

The general structure of the virtual corrections to the process $t \to W + b$ has been outlined in section 4.2. Here we will give results for the coefficients C_0^L, C_0^R, C_1^L and C_1^R that appear in the form factor decomposition, Eq. (4.10).

Integral function	Expression
$A_0(m_t)$	$m_t^2\left(\frac{1}{\epsilon}+\ln\frac{\mu^2}{m_t^2}+1\right)+O(\epsilon)$
$A_0(m_b)$	$m_b^2\left(\frac{1}{\epsilon}+\ln\frac{\mu^2}{m_t^2}+1-\ln\beta^2\right)+O(\epsilon)$
$B_0(p_t;0,m_t)$	$\frac{1}{\epsilon}+\ln\frac{\mu^2}{m_t^2}+2+O(\epsilon)$
$B_0(p_b;0,m_b)$	$\frac{1}{\epsilon}+\ln\frac{\mu^2}{m_t^2}+2-\ln(\beta^2)+O(\epsilon)$
$B_0(p_W;m_b,b_t)$	$\frac{1}{\epsilon}+\ln\frac{\mu^2}{m_t^2}+2+b^{(f)}+O(\epsilon)$
$C_0(p_b,p_t;0,m_b,m_t)$	$\frac{1}{2m_t^2\bar{P}_3}\left[\bar{Y}_p\left(\frac{1}{\epsilon}+\ln\frac{\mu^2}{m_t^2}\right)+c^{(f)}+O(\epsilon)\right]$

Table 6. Table of one-loop integrals obtained from ref. [43]. The functions $c^{(f)}$ and $b^{(f)}$ are given in the text.

These coefficients involve the following functions related to the scalar integrals,

$$\begin{aligned}
A_0(m_1) &= \frac{\mu^{4-D}}{i(2\pi)^D c_\Gamma}\int d^Dl\,\frac{1}{(l^2-m_1^2+i\varepsilon)}\,,\\
B_0(p_1;m_1,m_2) &= \frac{\mu^{4-D}}{i(2\pi)^D c_\Gamma}\int d^Dl\,\frac{1}{(l^2-m_1^2+i\varepsilon)((l+p_1)^2-m_2^2+i\varepsilon)}\,,\\
C_0(p_1,p_2;m_1,m_2,m_3) &= \frac{\mu^{4-D}}{i(2\pi)^D c_\Gamma}\int d^Dl\,\frac{1}{(l^2-m_1^2+i\varepsilon)((l+p_1)^2-m_2^2+i\varepsilon)((l+p_1+p_2)^2-m_3^2+i\varepsilon)}\,.
\end{aligned} \tag{B.4}$$

where the constant c_Γ has been defined in Eq. (4.11). Explicit expressions for the particular scalar integrals that appear in the calculation are given in Table 6. In order to have a compact representation for the finite parts of the integrals, we have introduced the following functions,

$$\begin{aligned}
b^{(f)} &= \frac{(1-\omega^2-\beta^2)}{\omega^2}\ln\beta+\frac{2\bar{P}_3}{\omega^2}\bar{Y}_p\,,\\
c^{(f)} &= \mathrm{Li}_2(1-\bar{P}_-)-\mathrm{Li}_2(1-\bar{P}_+)-\mathrm{Li}_2\left(1-\frac{\bar{P}_-}{\bar{P}_+}\right)+\ln^2\beta-\ln^2\bar{P}_+\,.
\end{aligned} \tag{B.5}$$

The results for the coefficients in the four-dimensional helicity scheme [44] are,

$$\begin{aligned}
C_0^L &= \left[\frac{\bar{P}_0}{\bar{P}_3}\bar{Y}_p-1\right]\frac{2}{\epsilon}+\frac{2\bar{P}_0}{\bar{P}_3}c^{(f)}-4+\ln(\beta^2)\\
&\quad+\frac{1}{2\bar{P}_3^2}b^{(f)}\left[1-\beta^2\omega^2-\omega^2+\beta^4-2\beta^2-6\bar{P}_3^2\right]-\frac{1}{2\bar{P}_3^2}\ln(\beta^2)\left[3\bar{P}_3^2+\beta^2\omega^2-\beta^4+\beta^2\right]\,,\\
C_0^R &= \frac{\beta}{\bar{P}_3^2}\left[\omega^2 b^{(f)}-\frac{1}{2}(1-\beta^2-\omega^2)\ln(\beta^2)\right]\,,\\
C_1^L &= \frac{\beta}{\bar{P}_3^2}\left[\bar{P}_0\ln(\beta^2)-\bar{W}_0 b^{(f)}\right]\,,\\
C_1^R &= \frac{1}{\bar{P}_3^2}\left[\frac{1}{2}(1-\omega^2-\beta^2)b^{(f)}-\beta^2\ln(\beta^2)\right]\,.
\end{aligned} \tag{B.6}$$

These expressions include the effects of wave function renormalization, as indicated in the upper-left diagram of Figure 6. The result in the four-dimensional helicity scheme is,

$$Z_Q = 1 - g^2 c_\Gamma C_F \left[\frac{3}{\epsilon} + 3\ln\left(\frac{\mu^2}{m^2}\right) + 5 \right] + O(g^4, \epsilon) \,. \tag{B.7}$$

The result for the wave function renormalization is independent of the gauge fixing parameter.

In terms of these coefficients the matrix element squared is,

$$\begin{aligned} &\mathcal{M}_\mu \mathcal{M}^*_\nu \left[-g^{\mu\nu} + \frac{p_W^\mu p_W^\nu}{m_W^2} \right] = \\ &\frac{2G_F m_t^4}{\sqrt{2}} \left\{ f + 2g^2 c_\Gamma \left(\frac{\mu^2}{m_t^2}\right)^\epsilon C_F \left[C_0^L f + (C_1^R + \beta C_1^L)(\frac{f}{2} - 3\omega^2 \bar{P}_0) - 6\beta\omega^2 C_0^R \right] \right\} + O(\alpha_S^2) \end{aligned} \tag{B.8}$$

Inserting the values for the coefficients from Eq. (B.6) and including the wave-function renormalization the total virtual result is,

$$\begin{aligned} \alpha_S \Gamma_1^{\rm virt} \;=\; & \Gamma_\infty \, 4 C_F g^2 c_\Gamma \left(\frac{\mu^2}{m_t^2}\right)^\epsilon \left[2f \left\{ \frac{1}{\epsilon} \left[\bar{P}_0 \bar{Y}_p - \bar{P}_3 \right] + \bar{P}_0 \Big[\mathrm{Li}_2(1-\bar{P}_-) - \mathrm{Li}_2(1-\bar{P}_+) - \mathrm{Li}_2\left(1 - \frac{\bar{P}_-}{\bar{P}_+}\right) \right. \right. \\ & \left. + \; \bar{Y}_p^2 - 2(\bar{Y}_p + \ln\beta)(\bar{Y}_w + \bar{Y}_p) + 2\bar{Y}_w \ln \bar{P}_+ \Big] - 2\bar{P}_3 \right\} \\ & + \; 12\omega^2 \bar{Y}_p \bar{P}_3^2 - \left[1 + 4\beta^2 - 5\beta^4 - \omega^2(5-\beta^2) + 4\omega^4 \right] \bar{P}_3 \ln\beta \Big] \,, \end{aligned} \tag{B.9}$$

in agreement with Czarnecki [20] after using standard identities between dilogarithms.

B.3 Real radiation

The evaluation of the real corrections relies on a factorization of the phase space into a simple form that is suited both to the calculation of the total width and the more differential calculations presented in this paper.

B.3.1 Factorization of Phase Space

For radiation in the decay the appropriate phase space is given by,

$$\begin{aligned} d\Phi^{(3)}(p_t; p_W, p_b, p_g) \;=\; & \frac{d^n p_W}{(2\pi)^{n-1}} \frac{d^n p_b}{(2\pi)^{n-1}} \frac{d^n p_g}{(2\pi)^{n-1}} \\ & \times \; \delta^+(p_W^2 - m_W^2) \delta^+(p_b^2 - m_b^2) \delta^+(p_g^2) (2\pi)^n \delta^n(p_t - p_W - p_b - p_g) \,. \end{aligned} \tag{B.10}$$

By inserting an integral over a delta function, $\delta^n(p_t - p_W - P) d^n P$, we can rewrite this in the familiar factorized form,

$$d\Phi^{(3)}(p_t; p_W, p_b, p_g) = \int \frac{dP^2}{2\pi} \, d\Phi^{(2)}(p_t; p_W, P) \, d\Phi^{(2)}(P; p_b, p_g) \,, \tag{B.11}$$

where $P = p_b + p_g$. Working in the center of mass frame of $P = p_b + p_g$ we have,

$$\begin{aligned} p_g \;&=\; \frac{m_t(z-\beta^2)}{2\sqrt{z}} (1, \ldots, \sin\theta, \cos\theta) \,, \\ p_b \;&=\; \frac{m_t(z+\beta^2)}{2\sqrt{z}} (1, \ldots, -v\sin\theta, -v\cos\theta) \,, \quad \text{with } v = \frac{z-\beta^2}{z+\beta^2} \,, \\ p_t \;&=\; (E_t, \ldots, 0, P_t) \,, \quad \text{with } E_t = \frac{m_t}{2\sqrt{z}}(1+z-\omega^2), \;\; P_t = \frac{m_t}{2\sqrt{z}} \sqrt{\lambda(1,\omega^2,z)} \,. \end{aligned} \tag{B.12}$$

Hence $P^2 = m_t^2 z$ and we can use the result of Eq. (B.1) to write the factorized form, Eq. (B.11), as,

$$d\Phi^{(3)}(p_t; p_W, p_b, p_g) = \frac{m_t^2}{2\pi} \int dz \, \frac{(4\pi)^{2\epsilon}}{32\pi^2} \frac{1}{(m_t^2)^\epsilon} \Big[\lambda(1,\omega^2,z)\Big]^{\frac{1}{2}-\epsilon} d^{n-2}\Omega_w \times \frac{(4\pi)^{2\epsilon}}{32\pi^2} \frac{1}{(m_t^2)^\epsilon} \, z^{-1+\epsilon}(z-\beta^2)^{1-2\epsilon} \, d^{n-2}\Omega_g \, . \tag{B.13}$$

By comparing Eq. (B.13) with the lowest order space space in Eq. (B.1) we can write the real emission phase space as a leading order normalization multiplying a term containing the real emission degrees of freedom,

$$d\Phi^{(3)}(p_t; p_W, p_b, p_g) = d\Phi^{(2)}(p_t; p_W, p_b) \times [dg(p_t, p_W, z)] \, . \tag{B.14}$$

The real emission factor factor $[dg(p_t, p_W, z)]$ is given by,

$$\begin{aligned}[dg(p_t, p_W, z)] &= \frac{(m_t^2)^{1-\epsilon}(4\pi)^{2\epsilon}}{64\pi^3} \int dz \Big[\frac{\lambda(1,\omega^2,z)}{\lambda(1,\omega^2,\beta^2)}\Big]^{\frac{1}{2}-\epsilon} z^{-1+\epsilon}(z-\beta^2)^{1-2\epsilon} \, d^{n-2}\Omega_g \\ &= c_\Gamma (m_t^2)^{1-\epsilon} \int dz \Big[\frac{\lambda(1,\omega^2,z)}{\lambda(1,\omega^2,\beta^2)}\Big]^{\frac{1}{2}-\epsilon} z^{-1+\epsilon}(z-\beta^2)^{1-2\epsilon} \left[\frac{4^\epsilon}{2}\int_{-1}^{1} dx (1-x^2)^{-\epsilon}\right] \end{aligned} \tag{B.15}$$

In this equation we have set $x = \cos\theta$ and c_Γ has been defined in Eq. (4.11).

B.3.2 Matrix element squared and integration.

We now present the result for the spin-averaged matrix element squared for the real radiation process, $t \to W + b + g$. The result is,

$$\begin{aligned}\mathcal{M}_\mu \mathcal{M}_\nu^* \Big(- g^{\mu\nu} + \frac{p_W^\mu p_W^\nu}{m_W^2}\Big) &= 2 g_s^2 C_F \frac{G_F m_t^4}{\sqrt{2}} \Bigg\{ f\left[-\frac{m_t^2}{p_t.p_g^2} - \frac{m_b^2}{p_b.p_g^2} + \frac{2m_t^2 \bar{P}_0}{p_t.p_g \, p_b.p_g}\right] \\ &+ f\left[\frac{2p_b.p_g - 2p_t.p_g}{p_t.p_g \, p_b.p_g}\right] + \frac{4\omega^2}{m_t^2}\frac{(p_t.p_g^2 + p_b.p_g^2)}{p_t.p_g \, p_b.p_g} + \frac{2(\beta^2+1)}{m_t^2}\frac{(p_t.p_g - p_b.p_g)^2}{p_t.p_g \, p_b.p_g}\Bigg\} \, . \end{aligned} \tag{B.16}$$

This expression can be written in terms of the variables of integration in the phase space measure, z and $x = \cos\theta$ (c.f. Eq (B.15)), by using the identities,

$$p_b.p_g = \frac{m_t^2}{2}(z-\beta^2) \qquad p_t.p_g = E_g(E_t - P_t\cos\theta) \, . \tag{B.17}$$

It is convenient to first perform the angular integration over $x = \cos\theta$. From the expression for the matrix element in Eq. (B.16) and the form of the phase space in Eq. (B.15), these integrations take the form,

$$J_n = \frac{4^\epsilon}{2}\int_{-1}^{1} dx \, (1-x^2)^{-\epsilon} \frac{1}{(p_t \cdot p_g)^n} \tag{B.18}$$

for $n = 0$, 1 and 2. The results for J_0, J_1 and J_2 are given in Table 7.

We shall first focus on the integration of the divergent terms appearing in the first set of parentheses [...] in Eq. (B.16). After performing the integration over x these terms lead to the following expressions, with the integral over z not yet evaluated. For the first term, containing the factor $m_t^2/(p_t.p_g)^2$, we are left with,

$$\begin{aligned} S_1 &= g^2 c_\Gamma C_F \left(\frac{\mu^2}{m_t^2}\right)^\epsilon \int_{\beta^2}^{z_m} dz \, z^{-\epsilon}\Big(\frac{z-\beta^2}{z}\Big)^{1-2\epsilon}\Big(\frac{\lambda(1,\omega^2,z)}{\lambda(1,\omega^2,\beta^2)}\Big)^{\frac{1}{2}-\epsilon}\frac{m_t^2}{E_g^2}\Big\{1 + 2\epsilon\frac{E_t}{P_t}Y_p + O(\epsilon^2)\Big\} \\ &= g^2 c_\Gamma C_F \left(\frac{\mu^2}{m_t^2}\right)^\epsilon \int_{\beta^2}^{z_m} dz \, \frac{4}{(z-\beta^2)^{1+2\epsilon}} z^\epsilon \Big(\frac{\lambda(1,\omega^2,z)}{\lambda(1,\omega^2,\beta^2)}\Big)^{\frac{1}{2}-\epsilon}\Big\{1 + 2\epsilon\frac{E_t}{P_t}Y_p + O(\epsilon^2)\Big\} \, . \end{aligned} \tag{B.19}$$

Integral	Result
J_0	$1+2\epsilon+O(\epsilon^2)$
J_1	$\frac{1}{E_g P_t}\Big\{Y_p+\epsilon\left[\mathrm{Li}_2\left(1-\frac{P_-}{P_+}\right)+Y_p^2\right]+O(\epsilon^2)\Big\}$
J_2	$\frac{1}{E_g^2 m_t^2}\Big\{1+2\epsilon\frac{E_t}{P_t}Y_p+O(\epsilon^2)\Big\}$

Table 7. Results for the angular integrations specified in Eq. (B.18).

The expression for the second term, with the factor $m_b^2/(p_b.p_g)^2$, is,

$$\begin{aligned} S_2 &= g^2 c_\Gamma C_F \left(\frac{\mu^2}{m_t^2}\right)^\epsilon \int_{\beta^2}^{z_m} dz\, z^{-\epsilon}\Big(\frac{z-\beta^2}{z}\Big)^{1-2\epsilon}\frac{4\beta^2}{(z-\beta^2)^2}\Big(\frac{\lambda(1,\omega^2,z)}{\lambda(1,\omega^2,\beta^2)}\Big)^{\frac{1}{2}-\epsilon}\Big\{1+2\epsilon+O(\epsilon^2)\Big\} \\ &= g^2 c_\Gamma C_F \left(\frac{\mu^2}{m_t^2}\right)^\epsilon \int_{\beta^2}^{z_m} dz\, \frac{4\beta^2}{(z-\beta^2)^{1+2\epsilon}} z^{-1+\epsilon}\Big(\frac{\lambda(1,\omega^2,z)}{\lambda(1,\omega^2,\beta^2)}\Big)^{\frac{1}{2}-\epsilon}\Big\{1+2\epsilon+O(\epsilon^2)\Big\}. \end{aligned} \tag{B.20}$$

The corresponding result for the third and final term, proportional to $\bar{P}_0/(p_t.p_g\; p_b.p_g)$, is,

$$\begin{aligned} S_3 &= -g^2 c_\Gamma C_F \left(\frac{\mu^2}{m_t^2}\right)^\epsilon \int_{\beta^2}^{z_m} dz\, z^{-\epsilon}\Big(\frac{z-\beta^2}{z}\Big)^{1-2\epsilon}\frac{2(1+\beta^2-\omega^2)}{(z-\beta^2)}\Big(\frac{\lambda(1,\omega^2,z)}{\lambda(1,\omega^2,\beta^2)}\Big)^{\frac{1}{2}-\epsilon}\frac{m_t^2}{E_g P_t} \\ &\times \Big\{Y_p+\epsilon\left[\mathrm{Li}_2\left(1-\frac{P_-}{P_+}\right)+Y_p^2\right]+O(\epsilon^2)\Big\} \\ &= -g^2 c_\Gamma C_F \left(\frac{\mu^2}{m_t^2}\right)^\epsilon \frac{8(1+\beta^2-\omega^2)}{\lambda(1,\beta,\omega^2)}\int_{\beta^2}^{z_m} dz\, z^\epsilon (z-\beta^2)^{-1-2\epsilon}\Big(\frac{\lambda(1,\omega^2,z)}{\lambda(1,\omega^2,\beta^2)}\Big)^{-\epsilon} \\ &\times \Big\{Y_p+\epsilon\left[\mathrm{Li}_2\left(1-\frac{P_-}{P_+}\right)+Y_p^2\right]+O(\epsilon^2)\Big\}. \end{aligned} \tag{B.21}$$

We may now perform the integration over z for each of these terms. For convenience we give useful results for the non-trivial integrands in Table 8. The notation is defined by,

$$\langle f(z)\rangle \equiv \int_{\beta^2}^{z_m} dz\, f(z)\,. \tag{B.22}$$

Performing the integrals in Eqs. (B.19), (B.20) and (B.21), using the results of Table 8, we obtain the following explicit results,

$$S_1 = -4g^2 c_\Gamma C_F \left(\frac{\mu^2}{m_t^2}\right)^\epsilon \left\{-\frac{1}{2\epsilon}-1+\ln\left(\frac{4\bar{P}_3^2}{\beta\omega}\right)-\bar{P}_0\frac{\bar{Y}_p}{\bar{P}_3}-\bar{W}_0\frac{\bar{Y}_w}{\bar{P}_3}\right\}, \tag{B.23}$$

$$S_2 = -4g^2 c_\Gamma C_F \left(\frac{\mu^2}{m_t^2}\right)^\epsilon \left\{-\frac{1}{2\epsilon}-1+\ln\left(\frac{4\bar{P}_3^2}{\beta\omega}\right)-(1-\omega^2)\frac{\bar{Y}_p}{\bar{P}_3}-\frac{1}{2}(1-\omega^2-\beta^2)\frac{\bar{Y}_w}{\bar{P}_3}\right\}, \tag{B.24}$$

$$\begin{aligned} S_3 &= 4g^2 c_\Gamma C_F \left(\frac{\mu^2}{m_t^2}\right)^\epsilon \frac{\bar{P}_0}{\bar{P}_3}\Big\{2\bar{Y}_p\Big[-\frac{1}{2\epsilon}+\ln\Big(\frac{4\bar{P}_3^2(z_m-\beta^2)}{\beta}\Big)\Big]+\mathrm{Li}_2(1-\bar{P}_-)-\mathrm{Li}_2(1-\bar{P}_+) \\ &- 3\,\mathrm{Li}_2\Big(1-\frac{\bar{P}_-}{\bar{P}_+}\Big)-3\,\bar{Y}_p^2+2\ln(\bar{P}_-)\ln(1-\omega-\bar{P}_-)-2\ln(\bar{P}_+)\ln(\bar{P}_+-1+\omega)\Big\}. \end{aligned} \tag{B.25}$$

$f(z)$	$\langle f(z)\rangle$
$\frac{1}{z-\beta^2}\ \left[Y_p(z)-\bar{Y}_p\right]$	$\bar{Y}_p\left(\ln(4\bar{P}_3^2)-\bar{Y}_p\right)+\frac{1}{2}\mathrm{Li}_2(1-\bar{P}_-)-\frac{1}{2}\mathrm{Li}_2(1-\bar{P}_+)$
	$-\mathrm{Li}_2(1-\frac{\bar{P}_-}{\bar{P}_+})+\ln(\bar{P}_-)\ln(1-\omega-\bar{P}_-)-\ln(\bar{P}_+)\ln(\bar{P}_+-1+\omega)$
$\frac{1}{z-\beta^2}\left[P_3(z)-\bar{P}_3\right]$	$\bar{P}_3\ln\left(\frac{4\bar{P}_3^2}{\omega(z_m-\beta^2)}\right)-\bar{P}_3-\bar{W}_0\bar{Y}_w$
$zY_p(z)$	$\frac{1}{4}\bar{P}_3(1+\beta^2+5\omega^2)-\frac{1}{2}\omega^2(2+\omega^2)\bar{Y}_w-\frac{1}{2}\beta^4\bar{Y}_p$
$Y_p(z)$	$\bar{P}_3-\omega^2\bar{Y}_w-\beta^2\bar{Y}_p$
$\frac{P_3(z)}{z^2}$	$-\frac{(1+\omega^2)}{1-\omega^2}\bar{Y}_p-\frac{\omega^2}{1-\omega^2}\bar{Y}_w+\frac{\bar{P}_3}{\beta^2}$
$\frac{P_3(z)}{z}$	$(1-\omega^2)\bar{Y}_p-\omega^2\bar{Y}_w-\bar{P}_3$
$P_3(z)$	$-\omega^2\bar{Y}_w+\bar{W}_0\bar{P}_3$

Table 8. Results for finite z integrals as defined in Eq. (B.22). Notation as in Table 1.

The remaining finite contributions can be integrated in four dimensions and added to the above results to yield the full real contribution to the width,

$$\begin{aligned}
\alpha_s\Gamma_1^{\text{real}} = \Gamma_\infty\, 4C_F g^2 c_\Gamma \left(\frac{\mu^2}{m_t^2}\right)^\epsilon \Big[2f\Big\{ &-\frac{1}{\epsilon}[\bar{P}_0\bar{Y}_p-\bar{P}_3]+\bar{P}_0\Big[\mathrm{Li}_2(1-\bar{P}_-)-\mathrm{Li}_2(1-\bar{P}_+)-3\,\mathrm{Li}_2(1-\frac{\bar{P}_-}{\bar{P}_+})\\
&-\bar{Y}_p^2+2(\bar{Y}_p+\ln(\beta))(\bar{Y}_w+\bar{Y}_p)+2\ln\left(\frac{4\bar{P}_3^2}{\bar{W}_+\bar{P}_+^2}\right)\bar{Y}_p\Big]+\Big[2+2\ln\left(\frac{\omega}{4\bar{P}_3^2}\right)\Big]\bar{P}_3\Big\}\\
&+2(1-\beta^2)\big[(1-\beta^2)^2+\omega^2(1+\beta^2)-4\omega^4\big]\bar{Y}_w\\
&+\frac{1}{2}\big[3-\beta^2+11\beta^4-\beta^6-4\beta^4\omega^2-9\omega^4+7\beta^2\omega^4+6\omega^6\big]\bar{Y}_p\\
&+4\big[1-2\beta^2+\beta^4+\omega^2+\beta^2\omega^2-2\omega^4\big]\bar{P}_3\ln(\beta)\\
&+\frac{1}{2}\big[5-22\beta^2+5\beta^4+9\omega^2(1+\beta^2)-6\omega^4\big]\bar{P}_3\Big]\,.
\end{aligned}\tag{B.26}$$

Adding in the virtual correction as given in Eq. (B.9) we find that the total correction to the width is in agreement with Eq. (2.6).

References

[1] J. M. Campbell and R. K. Ellis, *An update on vector boson pair production at hadron colliders*, *Phys. Rev.* **D60** (1999) 113006, [hep-ph/9905386].

[2] J. M. Campbell, R. K. Ellis, and F. Tramontano, *Single top production and decay at next-to-leading order*, *Phys.Rev.* **D70** (2004) 094012, [hep-ph/0408158].

[3] J. M. Campbell and R. K. Ellis, *MCFM for the Tevatron and the LHC*, *Nucl.Phys.Proc.Suppl.* **205-206** (2010) 10–15, [arXiv:1007.3492]. Talk presented by R.K Ellis at Loops and Legs in Quantum Field Theory 2010, Woerlitz, Germany, April 25-30, 2010.

[4] MCFM web page, *http://mcfm.fnal.gov/*, .

[5] P. Nason, S. Dawson, and R. K. Ellis, *The Total Cross-Section for the Production of Heavy Quarks in Hadronic Collisions*, *Nucl.Phys.* **B303** (1988) 607.

[6] T. M. Tait and C. Yuan, *The Phenomenology of single top quark production at the Fermilab Tevatron*, hep-ph/9710372.

[7] G. Bordes and B. van Eijk, *Calculating QCD corrections to single top production in hadronic interactions*, *Nucl.Phys.* **B435** (1995) 23–58.

[8] M. C. Smith and S. Willenbrock, *QCD and Yukawa corrections to single top quark production via* $q\bar{q} \to t\bar{b}$, *Phys.Rev.* **D54** (1996) 6696–6702, [hep-ph/9604223].

[9] T. Stelzer, Z. Sullivan, and S. Willenbrock, *Single top quark production via W - gluon fusion at next-to-leading order*, *Phys.Rev.* **D56** (1997) 5919–5927, [hep-ph/9705398].

[10] B. Harris, E. Laenen, L. Phaf, Z. Sullivan, and S. Weinzierl, *The Fully differential single top quark cross-section in next to leading order QCD*, *Phys.Rev.* **D66** (2002) 054024, [hep-ph/0207055].

[11] J. M. Campbell, R. Frederix, F. Maltoni, and F. Tramontano, *Next-to-Leading-Order Predictions for t-Channel Single-Top Production at Hadron Colliders*, *Phys.Rev.Lett.* **102** (2009) 182003, [arXiv:0903.0005].

[12] J. M. Campbell, R. Frederix, F. Maltoni, and F. Tramontano, *NLO predictions for t-channel production of single top and fourth generation quarks at hadron colliders*, *JHEP* **0910** (2009) 042, [arXiv:0907.3933].

[13] W. Bernreuther, A. Brandenburg, Z. Si, and P. Uwer, *Top quark pair production and decay at hadron colliders*, *Nucl.Phys.* **B690** (2004) 81–137, [hep-ph/0403035].

[14] K. Melnikov and M. Schulze, *NLO QCD corrections to top quark pair production and decay at hadron colliders*, *JHEP* **0908** (2009) 049, [arXiv:0907.3090].

[15] W. Bernreuther and Z.-G. Si, *Distributions and correlations for top quark pair production and decay at the Tevatron and LHC.*, *Nucl.Phys.* **B837** (2010) 90–121, [arXiv:1003.3926].

[16] K. Melnikov, A. Scharf, and M. Schulze, *Top quark pair production in association with a jet: QCD corrections and jet radiation in top quark decays*, *Phys.Rev.* **D85** (2012) 054002, [arXiv:1111.4991]. 22 pages, 8 figures.

[17] M. Jezabek and J. H. Kuhn, *QCD Corrections to Semileptonic Decays of Heavy Quarks*, *Nucl.Phys.* **B314** (1989) 1.

[18] G. Bevilacqua, M. Czakon, A. van Hameren, C. G. Papadopoulos, and M. Worek, *Complete off-shell effects in top quark pair hadroproduction with leptonic decay at next-to-leading order*, *JHEP* **1102** (2011) 083, [arXiv:1012.4230].

[19] R. Kleiss and W. Stirling, *Top quark production at hadron colliders: some useful formulae*, *Z.Phys.* **C40** (1988) 419–423.

[20] A. Czarnecki, *QCD corrections to the decay* $t \to Wb$ *in dimensional regularization*, *Phys.Lett.* **B252** (1990) 467–470.

[21] R. K. Ellis, D. Ross, and A. Terrano, *The Perturbative Calculation of Jet Structure in e+ e- Annihilation*, *Nucl.Phys.* **B178** (1981) 421.

[22] S. Catani and M. Seymour, *A General algorithm for calculating jet cross-sections in NLO QCD*, *Nucl.Phys.* **B485** (1997) 291–419, [hep-ph/9605323].

[23] A. Denner and T. Sack, *The Top width*, *Nucl.Phys.* **B358** (1991) 46–58.

[24] G. Eilam, R. Mendel, R. Migneron, and A. Soni, *Radiative corrections to top quark decay*, *Phys.Rev.Lett.* **66** (1991) 3105–3108.

[25] A. Czarnecki and K. Melnikov, *Two loop QCD corrections to top quark width*, *Nucl.Phys.* **B544** (1999) 520–531, [hep-ph/9806244].

[26] V. S. Fadin, V. A. Khoze, and A. D. Martin, *How suppressed are the radiative interference effects in heavy instable particle production?*, *Phys.Lett.* **B320** (1994) 141–144, [hep-ph/9309234].

[27] V. S. Fadin, V. A. Khoze, and A. D. Martin, *Interference radiative phenomena in the production of heavy unstable particles*, *Phys.Rev.* **D49** (1994) 2247–2256.

[28] K. Melnikov and O. I. Yakovlev, *Top near threshold: All alpha-S corrections are trivial*, *Phys.Lett.* **B324** (1994) 217–223, [hep-ph/9302311].

[29] R. Kleiss and W. Stirling, *Spinor Techniques for Calculating $p\bar{p} \to W^{\pm}/Z^0$ + Jets*, *Nucl.Phys.* **B262** (1985) 235–262.

[30] S. Badger, R. Sattler, and V. Yundin, *One-Loop Helicity Amplitudes for $t\bar{t}$ Production at Hadron Colliders*, *Phys.Rev.* **D83** (2011) 074020, [arXiv:1101.5947].

[31] J. Korner and Z. Merebashvili, *One loop corrections to four point functions with two external massive fermions and two external massless partons*, *Phys.Rev.* **D66** (2002) 054023, [hep-ph/0207054].

[32] G. Altarelli, R. K. Ellis, and G. Martinelli, *Large Perturbative Corrections to the Drell-Yan Process in QCD*, *Nucl.Phys.* **B157** (1979) 461.

[33] A. D. Martin, W. J. Stirling, R. S. Thorne, and G. Watt, *Parton distributions for the LHC*, *Eur. Phys. J.* **C63** (2009) 189–285, [arXiv:0901.0002].

[34] The CDF Collaboration, *Search for Standard Model Higgs Boson Production in Association with a W Boson with 9.45/fb of CDF Data*, . CDF Note 10796.

[35] **CMS Collaboration** Collaboration, S. Chatrchyan et al., *Measurement of the t-channel single top quark production cross section in pp collisions at sqrt(s) = 7 TeV*, *Phys.Rev.Lett.* **107** (2011) 091802, [arXiv:1106.3052].

[36] **CMS Collaboration** Collaboration, S. Chatrchyan et al., *Measurement of the $t\,\bar{t}$ Production Cross Section in pp Collisions at 7 TeV in Lepton + Jets Events Using b-quark Jet Identification*, *Phys.Rev.* **D84** (2011) 092004, [arXiv:1108.3773].

[37] **CDF** Collaboration, T. Aaltonen et al., *Evidence for a Mass Dependent Forward-Backward Asymmetry in Top Quark Pair Production*, *Phys. Rev.* **D83** (2011) 112003, [arXiv:1101.0034].

[38] The CDF Collaboration, *Measurement of the Forward Backward Asymmetry in Top Pair Production in the Dilepton Decay Channel using 5/fb*, . CDF Note 10436.

[39] **D0 Collaboration** Collaboration, V. M. Abazov et al., *Forward-backward asymmetry in top quark-antiquark production*, *Phys.Rev.* **D84** (2011) 112005, [arXiv:1107.4995].

[40] The CDF Collaboration, *Study of the Top Quark Production Asymmetry and Its Mass and Rapidity Dependence in the Full Run II Tevatron Dataset*, . CDF Note 10807.

[41] M. L. Mangano and S. J. Parke, *Multiparton amplitudes in gauge theories*, *Phys.Rept.* **200** (1991) 301–367, [hep-th/0509223].

[42] L. J. Dixon, *Calculating scattering amplitudes efficiently*, hep-ph/9601359.

[43] R. K. Ellis and G. Zanderighi, *Scalar one-loop integrals for QCD*, *JHEP* **0802** (2008) 002, [arXiv:0712.1851].

[44] Z. Bern, A. De Freitas, L. J. Dixon, and H. Wong, *Supersymmetric regularization, two loop QCD amplitudes and coupling shifts*, *Phys.Rev.* **D66** (2002) 085002, [hep-ph/0202271].